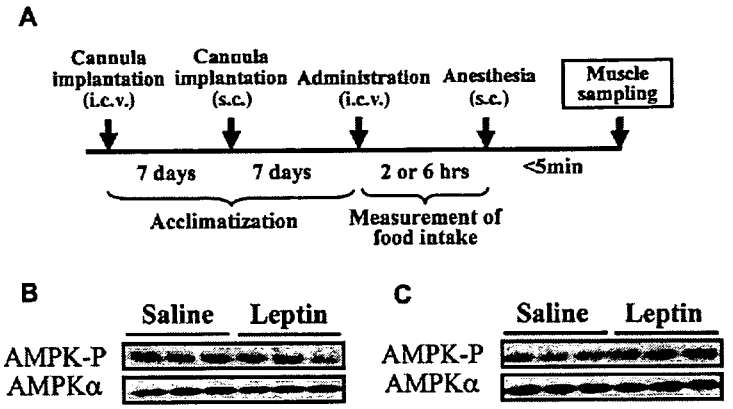

Figure 1. Establishment of the Experimental Protocol

(A) After intracerebroventricular (i.c.v.) and subcutaneous (s.c.) cannula implantation, mice were acclimatized and trained for handling. On the day of sampling, agents were administered i.c.v. in free-moving nonanesthetized mice. Food intake was measured and anesthesia was introduced s.c.

(B) Representative blots for phospho-AMPK and AMPKα in soleus muscle after leptin (0.5 μg) i.c.v. under intraperitoneal (i.p.) anesthesia. Muscles were sampled after another i.p. injection of the anesthetic agent.

(C) Representative blots for phospho-AMPK and AMPKα using the protocol in (A).

POMC is principally expressed in the arcuate nucleus of the hypothalamus (ARC) and the nucleus of the solitary tract (NTS) of the brainstem (Schwartz et al., 1997). The majority of POMC-expressing neurons in the ARC coexpress functional leptin receptor and mediate the anorectic effect of leptin (Cowley et al., 2001; Seeley et al., 1997). Although mouse models and human subjects with defective melanocortin signaling develop obesity (Huszar et al., 1997; Fan et al., 1997; Kobayashi et al., 2002; Farooqi et al., 2003), it remains largely unknown whether the central melanocortin system regulates fuel metabolism in skeletal muscle. In this context, we demonstrate here that the central melanocortin system is a critical mediator of leptin-induced skeletal muscle AMPK activation. In sharp contrast to leptin, melanocortin agonist retains its AMPK-activating potency even in mice fed a HFD.

RESULTS

Assessment of Skeletal Muscle AMPK Phosphorylation after Intracerebroventricular Administration in Conscious, Unrestrained Mice

AMPK activity is readily altered by various stimuli such as muscle contraction and ischemia (Hardie et al., 2006). To obtain reproducible results, establishment of an elaborately organized protocol was indispensable to minimize nonspecific AMPK activation. Intracerebroventricular (i.c.v.) and subcutaneous (s.c.) cannulae were implanted 14 and 7 days prior to the experiment, respectively, so that body weight recovered to the level of nonoperated mice on the sampling day (data not shown). Subcutaneous instead of intravenous cannulation was used to avoid a major weight loss. Agents were injected i.c.v. in well-acclimatized, nonanesthetized, free-moving mice. Anesthesia was introduced gently through s.c. cannula, and samples were obtained within 5 min (Figure 1A).

We first administered leptin i.c.v. under intraperitoneal (i.p.) anesthesia and sampled muscle after another i.p. injection of the anesthetic agent. By this method, we could not see a reproducible increase in phospho-AMPK levels by leptin (Figure 1B). In contrast, by the protocol in Figure 1A, leptin-induced increase in AMPK phosphorylation was clear (Figure 1C). In addition, we could also measure food intake, which was unaffected by anesthesia or by the nervousness of the mouse, precisely.

Melanocortin Agonist Increases AMPK Phosphorylation in Skeletal Muscle

Melanotan II (MT-II) is a potent melanocortin 3/4 receptor (MC3R/4R) agonist (Fan et al., 1997). Although it is known that central treatment with MT-II reduces food intake (Fan et al., 1997), its effect on skeletal muscle fuel metabolism has not been thoroughly addressed. We treated 8-week-old male C57BL/6 mice with leptin (0.5 μg) or MT-II (3.5 μg) i.c.v. and sampled the soleus muscle 6 hr later. Leptin i.c.v. significantly increased AMPK phosphorylation in the soleus muscle (Figure 2A). Likewise, MT-II i.c.v. increased phospho-AMPK levels by 69% ± 19% ($p < 0.05$ versus vehicle, $n = 7$). Neither leptin nor MT-II altered AMPKα protein levels, resulting in a 78% ± 14% ($p < 0.05$ versus vehicle, $n = 7$) and 64% ± 20% ($p < 0.05$ versus vehicle, $n = 7$) increase in phospho-AMPK/AMPKα ratio by leptin and MT-II, respectively (Figure 2A).

ACC is an established target of AMPK in muscle (Hardie et al., 2006). Phosphorylation of ACC by AMPK inhibits ACC enzyme activity and reduces the production of malonyl-CoA, thereby activating fatty acid β-oxidation (Minokoshi et al., 2002). In the present study, ACC phosphorylation was also augmented by MT-II by 90% ± 28% ($p < 0.05$ versus vehicle, $n = 7$) an increase comparable to that by leptin (83% ± 12%) ($p < 0.05$ versus vehicle, $n = 7$) (Figure 2B). Neither leptin nor MT-II i.c.v. altered ACC protein levels (see Figure S1A in the Supplemental Data available with this article online).

LepTg mice exhibit a more than 10-fold increase in plasma leptin levels, a paucity of adipose tissue, and enhanced glucose and lipid metabolism (Ogawa et al., 1999). In LepTg mice, soleus muscle AMPK phosphorylation and ACC phosphorylation were substantially increased compared with wild-type littermates (insets in Figures 2A and 2B). The levels of AMPK and ACC phosphorylation in MT-II or leptin i.c.v.-treated mice were comparable to those in LepTg mice.

AMPK phosphorylation was increased 2 hr after leptin i.c.v. by 63% ± 11% ($p < 0.05$ versus vehicle, $n = 7$) and maintained this level up to 6 hr (75% ± 10% increase)

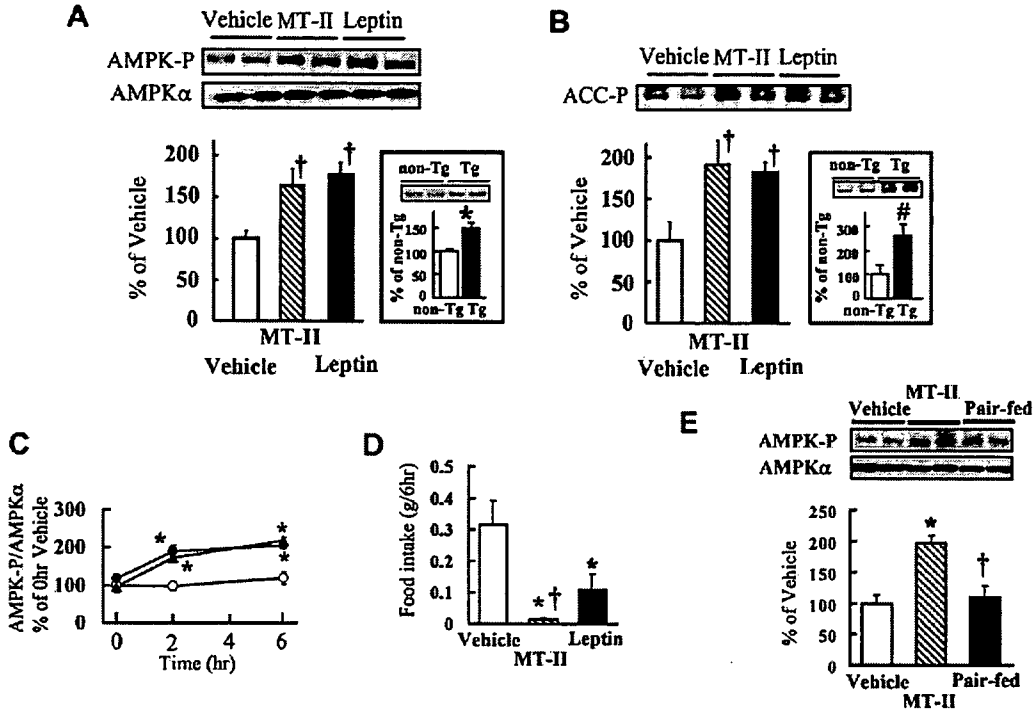

Figure 2. Increased Skeletal Muscle AMPK and ACC Phosphorylation after Intracerebroventricular MT-II Treatment

(A) Representative blots for phospho-AMPK and AMPKα in soleus muscle sampled 6 hr after MT-II (3.5 μg) or leptin (0.5 μg) i.c.v. The graph shows quantification of phospho-AMPK divided by that of AMPKα (phospho-AMPK/AMPKα ratio). †$p < 0.05$ versus vehicle, n = 7. Inset: Blots for phospho-AMPK and phospho-AMPK/AMPKα in LepTg mice. *$p < 0.05$ versus non-Tg, n = 6. In this and all other figures, error bars represent ± SEM.

(B) Representative blots for phospho-ACC in soleus muscle 6 hr after MT-II or leptin i.c.v. †$p < 0.05$ versus vehicle, n = 7. The graph shows the quantified data. Inset: Phospho-ACC in LepTg. #$p < 0.05$ versus non-Tg, n = 6.

(C) Phospho-AMPK/AMPKα before and 2 and 6 hr after MT-II or leptin i.c.v. ○, vehicle; ●, leptin; ▲, MT-II; *$p < 0.05$ versus vehicle, n = 6.

(D) Cumulative food intake over 6 hr. *$p < 0.05$ versus vehicle, †$p < 0.05$ versus leptin, n = 7.

(E) Blots for phospho-AMPK and AMPKα, and graph showing phospho-AMPK/AMPKα in MT-II-treated mice and vehicle-treated mice pair-fed with MT-II-treated counterparts. *$p < 0.05$ versus vehicle, †$p < 0.05$ versus MT-II, n = 6.

($p < 0.05$ versus vehicle, n = 7) (Figure 2C). Likewise, MT-II i.c.v. led to a significant increase in AMPK phosphorylation over 2 hr, by 100% ± 7% ($p < 0.05$ versus vehicle, n = 7), and this level was maintained until the 6 hr point (125% ± 12% increase) ($p < 0.05$ versus vehicle, n = 7) (Figure 2C). To determine whether increased AMPK phosphorylation is paralleled by any change in plasma glucose or insulin levels, mice were fasted for 3 hr, MT-II was injected i.c.v., and blood samples were obtained 6 hr later. No difference was observed in plasma glucose (vehicle 122 ± 12 mg/dl versus MT-II 125 ± 9 mg/dl; not significant [NS], n = 6) or insulin (vehicle 1.84 ± 0.10 ng/ml versus MT-II 1.77 ± 0.08 ng/ml; NS, n = 6) levels between vehicle- and MT-II-treated mice.

Leptin or MT-II i.c.v. suppressed food intake (Figure 2D). Over 6 hr, mice treated with leptin i.c.v. consumed 0.11 ± 0.05 g of food ($p < 0.05$ versus vehicle), while vehicle-treated mice consumed 0.32 ± 0.08 g. Mice treated with MT-II i.c.v. consumed 0.02 g with a standard deviation of less than 0.01 g ($p < 0.05$ versus vehicle, $p < 0.05$ versus leptin, n = 7). To rule out possible involvement of the anorectic effect of MT-II in increased AMPK phosphorylation in the muscle, we pair-fed vehicle-treated mice with mice treated with MT-II. In contrast to MT-II-treated mice, AMPK phosphorylation was not altered in the pair-fed mice ($p < 0.05$ versus vehicle, n = 6) (Figure 2E), showing that MT-II-induced AMPK phosphorylation is independent of suppression of food intake.

We next examined whether peripheral MT-II administration has a similar effect on skeletal muscle AMPK. We administered a single dose of MT-II (10 μg, s.c.) and examined AMPK and ACC phosphorylation 6 hr later. Peripheral treatment with MT-II at this dose also significantly increased AMPK (61% ± 19%) and ACC (69% ± 20%) phosphorylation compared with vehicle ($p < 0.05$ versus vehicle, n = 5) (data not shown).

Leptin-Induced AMPK and ACC Phosphorylation Is Attenuated by Melanocortin Antagonism

Leptin activates the hypothalamic melanocortin pathway (Schwartz et al., 1997; Cowley et al., 2001) and enhances skeletal muscle AMPK activity (Minokoshi et al., 2002). To test whether the central melanocortin system is involved in leptin-induced AMPK activation in the muscle, we injected

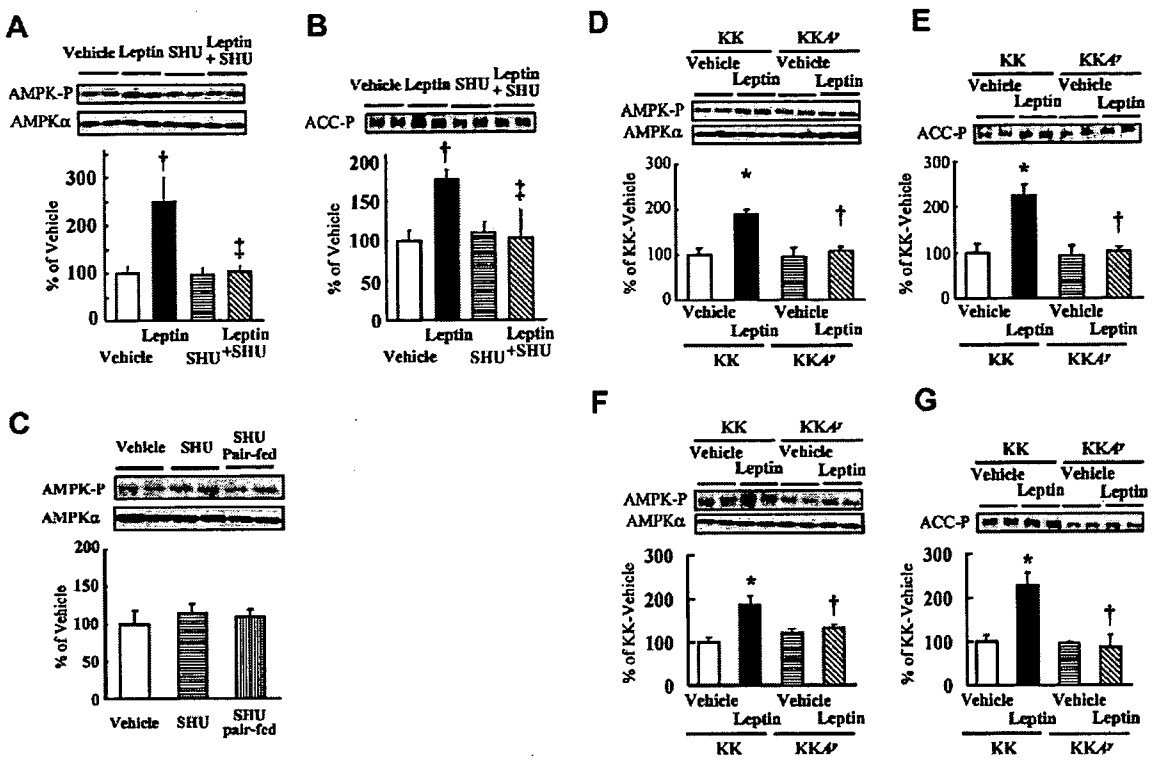

Figure 3. Attenuation of Leptin-Induced Muscle AMPK and ACC Phosphorylation by Pharmacologic or Genetic Melanocortin Blockade

(A, C, D, and F) Blots for phospho-AMPK and AMPKα, and graph showing phospho-AMPK/AMPKα.

(B, E, and G) Blots for phospho-ACC and quantified data.

Coadministration of SHU9119 (1.0 μg) i.c.v. attenuated leptin (0.5 μg)-induced increase in AMPK (A) and ACC (B) phosphorylation (†$p < 0.05$ versus vehicle, ‡$p < 0.05$ versus leptin, n = 7). Phospho-AMPK/AMPKα was not affected in mice treated with SHU9119 alone or in SHU9119-treated mice pair-fed with vehicle-treated mice (A and C). Leptin i.c.v. significantly increased AMPK (D and F) and ACC phosphorylation (E and G) in KK mice, while the increase was attenuated in both 6-week-old (D and E) and 10-week-old KKA^y mice (F and G) (*$p < 0.05$ versus KK-vehicle, †$p < 0.05$ versus KK-leptin, n = 6; data are % of KK-vehicle).

SHU9119, a MC3R/4R antagonist (Fan et al., 1997). Coadministration of SHU9119 i.c.v. (1.0 μg) suppressed leptin-induced increase in AMPK (Figure 3A) and ACC phosphorylation (Figure 3B) to the vehicle level (phospho-AMPK/AMPKα 150% ± 49% increase by leptin versus 4% ± 10% increase by leptin + SHU9119; phospho-ACC 79% ± 13% increase by leptin versus 6% ± 34% increase by leptin + SHU9119; $p < 0.05$, n = 7). Intracerebroventricular injection of SHU9119 alone did not affect AMPK (5% ± 9% decrease) or ACC (10% ± 12% increase) phosphorylation (Figures 3A and 3B). Central administration of SHU9119 alone or in conjunction with leptin did not change ACC protein levels (Figure S1B). SHU9119 i.c.v. significantly increased food intake over the following 6 hr (vehicle 0.35 ± 0.08 g versus SHU9119 0.49 ± 0.09 g; $p < 0.05$, n = 6). To test the hypothesis that increased food intake caused by SHU9119 may play a role in skeletal muscle AMPK regulation, we compared AMPK/ACC phosphorylation in vehicle-treated mice, SHU9119-treated mice, and SHU9119-treated mice pair-fed with vehicle-treated mice. Neither treatment with SHU9119 only nor treatment with SHU9119 plus pair-feeding had any effect on AMPK (SHU9119 15% ± 12% increase, SHU9119 plus pair-feeding 10% ± 10% increase versus vehicle) (Figure 3C) or ACC phosphorylation (SHU9119 8% ± 10% decrease, SHU9119 plus pair-feeding 13% ± 5% versus vehicle; NS, n = 6) (data not shown).

KKA^y mice (A^y mutants on a KK background) ectopically express agouti protein, an endogenous melanocortin receptor antagonist, throughout the body, including in the hypothalamus, and exhibit progressive obesity in addition to yellow coat color (Lu et al., 1994). Here we used preobese (6 weeks old, KK 29.0 ± 0.8 g versus KKA^y 29.1 ± 1.0 g; NS, n = 10) and obese (10 weeks old, KK 35.7 ± 1.4 g versus KKA^y 39.9 ± 1.0 g; $p < 0.05$, n = 14) male KKA^y mice to examine leptin-induced AMPK activation. The levels of AMPK and ACC phosphorylation were not significantly different between control KK and KKA^y mice at either age (Figures 3D–3G). Leptin i.c.v. led to a significant increase in AMPK (phospho-AMPK/AMPKα 90% ± 10% increase versus KK-vehicle; $p < 0.05$, n = 5) and ACC phosphorylation (125% ± 25% increase versus

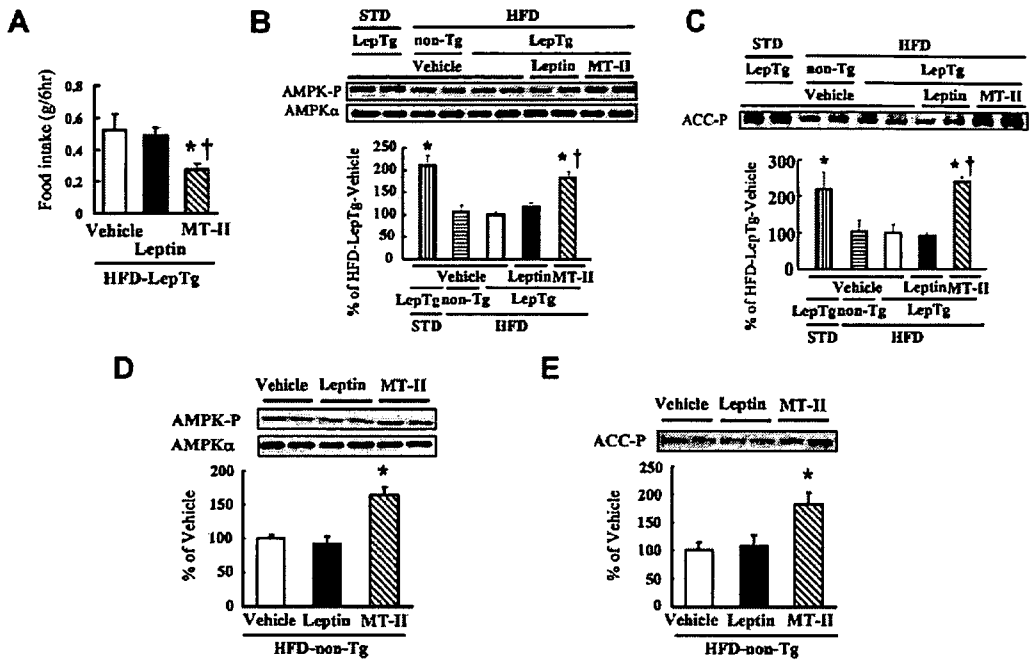

Figure 4. Recovery of Skeletal Muscle AMPK and ACC Phosphorylation by Intracerebroventricular MT-II Treatment in Mice Fed a High-Fat Diet

(A) Food intake over the 6 hr after i.c.v. injection in HFD-LepTg mice. *$p < 0.05$ versus vehicle, †$p < 0.05$ versus leptin, $n = 7$.

(B and D) Blots for phospho-AMPK and AMPKα, and graph showing phospho-AMPK/AMPKα ratio.

(C and E) Blots for phospho-ACC and quantified data.

(B–E) In HFD-LepTg mice, AMPK phosphorylation (B) and ACC phosphorylation (C) were decreased in comparison to STD-LepTg mice and were comparable to HFD-non-Tg mice. In HFD-LepTg mice, leptin i.c.v. did not alter AMPK (B) or ACC phosphorylation (C). MT-II (3.5 μg) i.c.v. restored AMPK (B) and ACC phosphorylation (C) in HFD-LepTg mice (*$p < 0.05$ versus HFD-LepTg-vehicle, †$p < 0.05$ versus HFD-LepTg-leptin, $n = 7$; data are % of HFD-LepTg vehicle) and HFD-non-Tg mice (D and E) (*$p < 0.05$ versus HFD-non-Tg-vehicle, $n = 5$).

KK-vehicle, $p < 0.05$, $n = 5$) in 6-week-old KK mice, while the increase was attenuated in 6-week-old KKA^y mice (phospho-AMPK/AMPKα 15% ± 21% increase, phospho-ACC 10% ± 11% increase; $p < 0.05$ versus KK-leptin, $n = 5$) (Figures 3D and 3E). ACC protein levels were not different between 6-week-old KK and KKA^y mice (Figure S1C). The results were similar in 10-week-olds, with a significant leptin-induced increase in AMPK (phospho-AMPK/AMPKα 85% ± 17% increase versus KK-vehicle; $p < 0.05$, $n = 7$) and ACC phosphorylation (133% ± 28% increase versus KK-vehicle; $p < 0.05$, $n = 7$) in KK mice and a lack of change in KKA^y mice by leptin (phospho-AMPK/AMPKα 18% ± 3% increase, phospho-ACC 21% ± 32% decrease; $p < 0.05$ versus KK-leptin, $n = 7$) (Figures 3F and 3G).

Central Treatment with MT-II Leads to Recovery of HFD-Induced Attenuation in AMPK and ACC Phosphorylation

LepTg mice exhibit decreased caloric intake and increased energy expenditure (Ogawa et al., 1999; Tanaka et al., 2005). Enhanced glucose tolerance, increased insulin sensitivity, and lower plasma triglyceride in LepTg mice are independent of reduced food intake (Ogawa et al., 1999). Over 4 weeks on HFD, LepTg mice, which remain significantly more hyperleptinemic than non-Tg mice (176 ± 4 versus 78 ± 7 ng/ml), become as obese, glucose intolerant, insulin resistant, and hyperlipidemic as non-Tg mice (Tanaka et al., 2005). Muscle AMPK/ACC phosphorylation is also attenuated (Tanaka et al., 2005).

To address the effect of central melanocortin activation under HFD, we treated HFD-LepTg mice with MT-II. MT-II i.c.v., but not leptin i.c.v., suppressed food intake in HFD-LepTg mice (vehicle 0.52 ± 0.10 g, leptin 0.49 ± 0.05 g, MT-II 0.28 ± 0.04 g; MT-II $p < 0.05$ versus vehicle or leptin, $n = 7$) (Figure 4A). In HFD-LepTg mice, muscle AMPK phosphorylation and ACC phosphorylation were significantly decreased compared with STD-LepTg mice and were comparable to HFD-non-Tg mice (Figures 4B and 4C). Of note, leptin i.c.v. in addition to transgenic hyperleptinemia did not augment AMPK (21% ± 14% increase, NS) or ACC phosphorylation (8% ± 6% decrease, NS) in HFD-LepTg mice (Figures 4B and 4C). In contrast, MT-II i.c.v. effectively augmented AMPK (by 85% ± 13%; $p < 0.05$ versus HFD-LepTg vehicle) and ACC phosphorylation (by 139% ± 16%; $p < 0.05$ versus HFD-LepTg vehicle) in HFD-LepTg mice (Figures 4B and 4C), suggesting that MT-II is a potent AMPK activator in muscle even under HFD. To confirm the results with LepTg mice, we treated HFD-fed wild-type (non-Tg) mice with leptin or MT-II

i.c.v. As expected, MT-II i.c.v., but not leptin i.c.v., led to a significant increase in muscle AMPK (leptin 8% ± 10% decrease, NS; MT-II 64% ± 12% increase versus vehicle; $p < 0.05$, $n = 5$) (Figure 4D) and ACC phosphorylation (leptin 19% ± 25% increase, NS; MT-II 96% ± 20% increase versus vehicle; $p < 0.05$, $n = 5$) (Figure 4E) in the wild-type mice. ACC expression was not altered by HFD or by HFD plus leptin or MT-II i.c.v. (Figure S1D).

DISCUSSION

Despite vigorous research, the question of why leptin loses its lipid-mobilizing potency under HFD has not been fully answered. Hypothalamic and peripheral induction of SOCS-3 (Bjorbaek et al., 1998; Howard et al., 2004; Wang et al., 2005; Kievit et al., 2006) and decreased permeability of the blood-brain barrier (El-Haschimi et al., 2000; Oh-I et al., 2005) have been implicated in attenuated leptin receptor signaling and metabolic efficacy. A recent study has demonstrated blunted hypothalamic AMPK as well as STAT3 signaling in HFD-fed mice (Martin et al., 2006). In the present study, neither transgenic hyperleptinemia nor central leptin treatment increased skeletal muscle AMPK phosphorylation under HFD. Notably, however, central MT-II administration did increase skeletal muscle AMPK phosphorylation in mice fed a HFD, indicating a mechanism upstream of the central melanocortin system that is responsible for the leptin resistance.

AMPK is a cellular fuel gauge activated by a variety of stresses. To stably assess AMPK activity in skeletal muscle, samples must be obtained quickly and deliberately. Furthermore, surgical interventions such as i.c.v. or intravenous cannulation cause substantial weight loss during the following week, making it more difficult to interpret the results in terms of energy homeostasis. In this sense, implementation of our devised protocol was instrumental in showing that skeletal muscle AMPK phosphorylation is regulated by the central melanocortin system. Phosphorylation of the α subunit of AMPK at Thr172 is tightly correlated with AMPK activity in many experimental conditions, including leptin-induced AMPK activation in the skeletal muscle (Minokoshi et al., 2002). Increased phosphorylation of AMPK and ACC in parallel firmly suggests increased AMPK activity in vivo.

In contrast to the effects of the central melanocortin system on satiety, little is known about its impact on fuel metabolism in the peripheral tissues. A recent study has shown that MT-II i.c.v. increases basal and insulin-stimulated glucose disposal and basal hepatic glucose production (Heijboer et al., 2005). However, MT-II does not seem to alter insulin-dependent suppression of hepatic glucose production (Heijboer et al., 2005). Our data here demonstrate that the administration of melanocortin agonist augments skeletal muscle AMPK and ACC phosphorylation. Considering the crucial role of skeletal muscle AMPK in the regulation of fatty acid β-oxidation (Minokoshi et al., 2002), our data strongly suggest a metabolic link between the central melanocortin system and skeletal muscle fatty acid mobilization. On the other hand, we did not observe any change in fasting plasma glucose or insulin levels 6 hr after MT-II i.c.v. Heijboer et al. (2005) also report an absence of change in basal plasma glucose and insulin levels following MT-II i.c.v. Further studies utilizing a combination of glucose clamp and measurement of AMPK activity may give a more accurate view of the temporal relationships between AMPK activation and skeletal muscle glucose utilization. POMC neurons are chiefly present in the ARC and NTS, while MC4R, a major melanocortin receptor involved in energy homeostasis, is widely distributed and present in the paraventricular hypothalamic nucleus (PVN) and the dorsal motor nucleus of the vagus (DMV) (Liu et al., 2003). Further studies are necessary to specify which nuclei within the central melanocortin system mediate skeletal muscle AMPK activation.

Leptin is a pleiotropic hormone, serving as a critical regulator of energy homeostasis, reproduction, blood pressure, and bone metabolism (Masuzaki et al., 1997; Aizawa-Abe et al., 2000; Ducy et al., 2000). Although a crucial role of the hypothalamic melanocortin system has been recognized in the anorexigenic effect of leptin, the matter of which functions of leptin are melanocortin dependent or independent still remains controversial. We previously reported that hypertension in LepTg mice is not ameliorated by SHU9119 i.c.v., implicating a melanocortin-independent pathway in blood pressure control by leptin (Aizawa-Abe et al., 2000). In terms of effects on glucose homeostasis, a recent study has shown that enhancement in hepatic gluconeogenesis by leptin is blocked by SHU9119 i.c.v., whereas leptin-dependent reduction in glycogenolysis is not (Gutierrez-Juarez et al., 2004). Taking these previous studies together, it is reasonable to postulate that metabolic regulation by leptin is mediated by both melanocortin-dependent and -independent pathways. Here we show that pharmacological (SHU9119) or genetic (KKA^y) blockade of the melanocortin receptor attenuates leptin-dependent AMPK and ACC phosphorylation. These data provide evidence that the leptin-skeletal muscle AMPK axis is mediated by the central melanocortin system.

Leptin-induced augmentation of AMPK and ACC phosphorylation was attenuated in both 6-week-old and 10-week-old KKA^y mice. In 10-week-old obese KKA^y mice, decreased AMPK response to leptin may be partly attributable to the secondary effect of obesity. However, absence of muscle AMPK activation was observed even in lean 6-week-old KKA^y mice, further supporting the notion that melanocortin signaling is necessary for leptin-induced AMPK activation. In KKA^y mice, skeletal muscle phospho-AMPK levels were not altered compared with KK mice despite reported hyperphagia (Fan et al., 1997). Central administration of SHU9119 alone also causes hyperphagia (Fan et al., 1997) but did not alter skeletal muscle AMPK phosphorylation in our present study. The discrepancy between food intake and AMPK phosphorylation may suggest diverging pathways regulating satiety and skeletal muscle AMPK activity.

A recent study has shown that peripheral, but not central, administration of ciliary neurotrophic factor (CNTF), another potent anorectic agent in HFD-fed mice, activates

skeletal muscle AMPK (Watt et al., 2006). Although CNTF, like leptin, increases phospho-STAT3 in the ARC, the anorectic effect of CNTF remains intact in *Mc4r* knockout mice (Marsh et al., 1999). Noting that the anorectic effect of leptin is substantially attenuated in *Mc4r* knockouts (Marsh et al., 1999), these data suggest that central signaling cascades of leptin and CNTF are independent at the level of the melanocortin system and that centrally mediated AMPK activation in muscle is unique to the leptin-melanocortin pathway.

A previous work (Pierroz et al., 2002) and ours here demonstrate that MT-II suppresses food intake in mice fed a HFD. Another paper published recently has shown that leptin-induced α-MSH secretion from the ARC is abrogated in obese mice fed a HFD (Enriori et al., 2007). In the Enriori et al. study, the authors also showed that *Mc4r* expression is reciprocally upregulated in PVN from obese mice. These data further support our results showing that MT-II remains effective in suppressing food intake and activating skeletal muscle AMPK even under HFD. Taken together, our findings reinforce the notion that MT-II may be beneficial for the treatment of insulin resistance, a pathology characterized by a myocellular lipid excess. However, since the results of the present study are based mainly on data from i.c.v. injections, further studies are necessary to explore the clinical efficacy of melanocortin agonists.

In conclusion, our data demonstrate that leptin-induced skeletal muscle AMPK activation is at least partly mediated by the central melanocortin system. In contrast to leptin, AMPK activation by melanocortin agonist is preserved even under HFD. Our data provide an insight into the central regulation of skeletal muscle AMPK activity and suggest a possible recovery of skeletal muscle fatty acid β-oxidation by melanocortin agonists under dietary lipid overload.

EXPERIMENTAL PROCEDURES

Animal Experiments

C57BL/6 (B6), KK, and KKA^y mice were obtained from CLEA Japan. Heterozygous LepTg and non-Tg littermates on a B6 background (Ogawa et al., 1999) were used. Animals were maintained on STD (F-2, 3.7 kcal/g, 12% of kcal from fat, source soybean, Funahashi Farm) and a 14 hr light/10 hr dark cycle at 23°C. HFD was from Research Diets (D12493, 5.2 kcal/g, 60% of kcal from fat, source soybean/lard). Animals were given free access to food and water unless otherwise mentioned. Body weight and food intake were monitored for the animals' well-being. Experiments were started between 6 and 8 weeks of age, except for KK and KKA^y experiments. HFD was administered for 4 weeks. Cannulae (Plastics One) were inserted stereotactically into lateral ventricles and fixed. On the sampling day, leptin (0.5 μg), MT-II (3.5 μg), SHU9119 (1.0 μg), or a combination was administered in 0.5 μl saline solution at around the start of the light period. The weight of the food pellet at the start and at the end of the experiment was measured with a microbalance (A&D). Five to ten g/kg chloral hydrate (Nakalai Tesque) was administered through s.c. cannula (PE20, Becton Dickinson) 2 or 6 hr after i.c.v. injection, and the soleus muscle was sampled. Successful i.c.v. delivery of the reagents was ensured by injecting dye to every animal postmortem and omitting data from those with inadequate distribution of the dye. Plasma glucose and insulin levels were measured by Glucose C-II Test Wako (Wako Pure Chemical Industries) and Insulin ELISA Kit (Morinaga). Animal experiments were performed in accordance with the Kyoto University guidelines for animal experiments and were approved by the Animal Research Committee, Kyoto University Graduate School of Medicine.

Western Blots

Muscle samples were homogenized as described (Tanaka et al., 2005). After denaturing, 15 μg per lane of protein was loaded on 10% and 4%–20% SDS-polyacrylamide gels for AMPK and ACC, respectively, and transferred to PVDF membrane (PerkinElmer). Phosphospecific antibodies were used for the detection of phospho-AMPK and phospho-ACC. Antibodies were anti-phospho-Thr172 AMPKα, anti-AMPKα (Cell Signaling Technology), and anti-phospho-Ser79 ACC (Upstate). ECL Plus (Amersham), a LAS-1000 image analyzer, and MultiGauge version 2.0 (Fujifilm) were used for detection and quantification.

Statistical Analyses

Data are presented as means ± SEM. Comparisons between or among animal groups were performed by Student's t test or repeated analysis of variance (ANOVA), where applicable, and completed by Fisher's probable least-significant-difference test.

Supplemental Data

Supplemental Data include one figure and can be found with this article online at http://www.cellmetabolism.org/cgi/content/full/5/5/395/DC1/.

ACKNOWLEDGMENTS

We thank M. Nagamoto, S. Masumoto, K. Takahashi, S. Maki, K. Koyama, A. Yumoto, S. Kozuka, H. Managi, and K. Shiiya for assistance. This work was supported by MEXT Grants-in-Aid B2:16390267, S2:16109007, B:18790634, and adipomics:15081101; a MHLW Health and Labor Science Research Grant; and grants from JST, AstraZeneca, the Takeda Medical Research Foundation, the Smoking Research Foundation, Metabolic Syndrome Foundation, the Japan Foundation for Applied Enzymology, and NCVC.

Received: September 25, 2006
Revised: January 22, 2007
Accepted: April 17, 2007
Published: May 8, 2007

REFERENCES

Aizawa-Abe, M., Ogawa, Y., Masuzaki, H., Ebihara, K., Satoh, N., Iwai, H., Matsuoka, N., Hayashi, T., Hosoda, K., Inoue, G., et al. (2000). Pathophysiological role of leptin in obesity-related hypertension. J. Clin. Invest. *105*, 1243–1252.

Bjorbaek, C., Elmquist, J.K., Frantz, J.D., Shoelson, S.E., and Flier, J.S. (1998). Identification of SOCS-3 as a potential mediator of central leptin resistance. Mol. Cell *1*, 619–625.

Cowley, M.A., Smart, J.L., Rubinstein, M., Cerdan, M.G., Diano, S., Horvath, T.L., Cone, R.D., and Low, M.J. (2001). Leptin activates anorexigenic POMC neurons through a neural network in the arcuate nucleus. Nature *411*, 480–484.

Ducy, P., Amling, M., Takeda, S., Priemel, M., Schilling, A.F., Beil, F.T., Shen, J., Vinson, C., Rueger, J.M., and Karsenty, G. (2000). Leptin inhibits bone formation through a hypothalamic relay: a central control of bone mass. Cell *100*, 197–207.

Ebihara, K., Kusakabe, T., Hirata, M., Masuzaki, H., Miyanaga, F., Kobayashi, N., Tanaka, T., Chusho, H., Miyazawa, T., Hayashi, T., et al. (2007). Efficacy and safety of leptin-replacement therapy and possible mechanisms of leptin actions in patients with generalized lipodystrophy. J. Clin. Endocrinol. Metab. *92*, 532–541.

El-Haschimi, K., Pierroz, D.D., Hileman, S.M., Bjorbaek, C., and Flier, J.S. (2000). Two defects contribute to hypothalamic leptin resistance in mice with diet-induced obesity. J. Clin. Invest. *105*, 1827–1832.

Enriori, P.J., Evans, A.E., Sinnayah, P., Jobst, E.E., Tonelli-Lemos, L., Billes, S.K., Glavas, M.M., Grayson, B.E., Perello, M., Nillni, E.A., et al. (2007). Diet-induced obesity causes severe but reversible leptin resistance in arcuate melanocortin neurons. Cell Metab. *5*, 181–194.

Fan, W., Boston, B.A., Kesterson, R.A., Hruby, V.J., and Cone, R.D. (1997). Role of melanocortinergic neurons in feeding and the agouti obesity syndrome. Nature *385*, 165–168.

Farooqi, S.I., Keogh, J.M., Yeo, G.S.H., Lank, E.J., Cheetham, T., and O'Rahilly, S. (2003). Clinical spectrum of obesity and mutations in the melanocortin 4 receptor gene. N. Engl. J. Med. *348*, 1085–1095.

Gutierrez-Juarez, R., Obici, S., and Rossetti, L. (2004). Melanocortin-independent effects of leptin on hepatic glucose fluxes. J. Biol. Chem. *279*, 49704–49715.

Hardie, D.G., Hawley, S.A., and Scott, J.W. (2006). AMP-activated protein kinase- development of the energy sensor concept. J. Physiol. *574*, 7–15.

Heijboer, A.C., van den Hoek, A.M., Pijl, H., Voshol, P.J., Havekes, L.M., Romijn, J.A., and Corssmit, E.P. (2005). Intracerebroventricular administration of melanotan II increases insulin sensitivity of glucose disposal in mice. Diabetologia *48*, 1621–1626.

Howard, J.K., Cave, B.J., Oksanen, L.J., Tzameli, I., Bjorbaek, C., and Flier, J.S. (2004). Enhanced leptin sensitivity and attenuation of diet-induced obesity in mice with haploinsufficiency of Socs3. Nat. Med. *10*, 734–738.

Huszar, D., Lynch, C.A., Fairchild-Huntress, V., Dunmore, J.H., Fang, Q., Berkemeier, L.R., Gu, W., Kesterson, R.A., Boston, B.A., Cone, R.D., et al. (1997). Targeted disruption of the melanocortin-4 receptor results in obesity in mice. Cell *88*, 131–141.

Kievit, P., Howard, J.K., Badman, M.K., Balthasar, N., Coppari, R., Mori, H., Lee, C.E., Elmquist, J.K., Yoshimura, A., and Flier, J.S. (2006). Enhanced leptin sensitivity and improved glucose homeostasis in mice lacking suppressor of cytokine signaling-3 in POMC-expressing cells. Cell Metab. *4*, 123–132.

Kobayashi, H., Ogawa, Y., Shintani, M., Ebihara, K., Shimodahira, M., Iwakura, T., Hino, M., Ishihara, T., Ikekubo, K., Kurahachi, H., et al. (2002). A novel homozygous missense mutation of melanocortin-4 receptor (MC4R) in a Japanese woman with severe obesity. Diabetes *51*, 243–246.

Liu, H., Kishi, T., Roseberry, A.G., Cai, X., Lee, C.E., Montez, J.M., Friedman, J.M., and Elmquist, J.K. (2003). Transgenic mice expressing green fluorescent protein under the control of the melanocortin-4 receptor promoter. J. Neurosci. *23*, 7143–7154.

Lu, D., Willard, D., Patel, I.R., Kadwell, S., Overton, L., Kost, T., Luther, M., Chen, W., Woychik, R.P., Wilkison, W.O., et al. (1994). Agouti protein is an antagonist of the melanocyte-stimulating-hormone receptor. Nature *371*, 799–802.

Maffei, M., Halaas, J., Ravussin, E., Pratley, R.E., Lee, G.H., Zhang, Y., Fei, H., Kim, S., Lallone, R., Ranganathan, S., et al. (1995). Leptin levels in human and rodent: Measurement of plasma leptin and ob RNA in obese and weight-reduced subjects. Nat. Med. *1*, 1155–1161.

Marsh, D.J., Hollopeter, G., Huszar, D., Laufer, R., Yagaloff, K.A., Fisher, S.L., Burn, P., and Palmiter, R.D. (1999). Response of melanocortin-4 receptor-deficient mice to anorectic and orexigenic peptides. Nat. Genet. *21*, 119–122.

Martin, T.L., Alquier, T., Asakura, K., Furukawa, N., Preitner, F., and Kahn, B.B. (2006). Diet-induced obesity alters AMP kinase activity in hypothalamus and skeletal muscle. J. Biol. Chem. *281*, 18933–18941.

Masuzaki, H., Ogawa, Y., Sagawa, N., Hosoda, K., Matsumoto, T., Mise, H., Nishimura, H., Yoshimasa, Y., Tanaka, I., Mori, T., et al. (1997). Nonadipose tissue production of leptin: leptin as a novel placenta-derived hormone in humans. Nat. Med. *3*, 1029–1033.

Minokoshi, Y., Kim, Y.B., Peroni, O.D., Fryer, L.G., Muller, C., Carling, D., and Kahn, B.B. (2002). Leptin stimulates fatty-acid oxidation by activating AMP-activated protein kinase. Nature *415*, 339–343.

Ogawa, Y., Masuzaki, H., Hosoda, K., Aizawa-Abe, M., Suga, J., Suda, M., Ebihara, K., Iwai, H., Matsuoka, N., Satoh, N., et al. (1999). Increased glucose metabolism and insulin sensitivity in transgenic skinny mice overexpressing leptin. Diabetes *48*, 1822–1829.

Oh-I, S., Shimizu, H., Sato, T., Uehara, Y., Okada, S., and Mori, M. (2005). Molecular mechanisms associated with leptin resistance: n-3 polyunsaturated fatty acids induce alterations in the tight junction of the brain. Cell Metab. *1*, 331–341.

Oral, E.A., Simha, V., Ruiz, E., Andewelt, A., Premkumar, A., Snell, P., Wagner, A.J., Depaoli, A.M., Reitman, M.L., Taylor, S.I., et al. (2002). Leptin-replacement therapy for lipodystrophy. N. Engl. J. Med. *346*, 570–578.

Pierroz, D.D., Ziotopoulou, M., Ungsunan, L., Moschos, S., Flier, J.S., and Mantzoros, C.S. (2002). Effects of acute and chronic administration of the melanocortin agonist MTII in mice with diet-induced obesity. Diabetes *51*, 1337–1345.

Schwartz, M.W., Seeley, R.J., Woods, S.C., Weigle, D.S., Campfield, L.A., Burn, P., and Baskin, D.G. (1997). Leptin increases hypothalamic pro-opiomelanocortin mRNA expression in the rostral arcuate nucleus. Diabetes *46*, 2119–2123.

Seeley, R.J., Yagaloff, K.A., Fisher, S.L., Burn, P., Thiele, T.E., van Dijk, G., Baskin, D.G., and Schwartz, M.W. (1997). Melanocortin receptors in leptin effects. Nature *390*, 349.

Shimabukuro, M., Koyama, K., Chen, G., Wang, M.Y., Trieu, F., Lee, Y., Newgard, C.B., and Unger, R.H. (1997). Direct antidiabetic effect of leptin through triglyceride depletion of tissues. Proc. Natl. Acad. Sci. USA *94*, 4637–4641.

Tanaka, T., Hidaka, S., Masuzaki, H., Yasue, S., Minokoshi, Y., Ebihara, K., Chusho, H., Ogawa, Y., Toyoda, T., Sato, K., et al. (2005). Skeletal muscle AMP-activated protein kinase phosphorylation parallels metabolic phenotype in leptin transgenic mice under dietary modification. Diabetes *54*, 2365–2374.

Wang, M.Y., Orci, L., Ravazzola, M., and Unger, R.H. (2005). Fat storage in adipocytes requires inactivation of leptin's paracrine activity: implications for treatment of human obesity. Proc. Natl. Acad. Sci. USA *102*, 18011–18016.

Watt, M.J., Dzamko, N., Thomas, W.G., Rose-John, S., Ernst, M., Carling, D., Kemp, B.E., Febbraio, M.A., and Steinberg, G.R. (2006). CNTF reverses obesity-induced insulin resistance by activating skeletal muscle AMPK. Nat. Med. *12*, 541–548.

Pathway for Differentiation of Human Embryonic Stem Cells to Vascular Cell Components and Their Potential for Vascular Regeneration

Masakatsu Sone, Hiroshi Itoh, Kenichi Yamahara, Jun K. Yamashita, Takami Yurugi-Kobayashi, Akane Nonoguchi, Yutaka Suzuki, Ting-Hsing Chao, Naoki Sawada, Yasutomo Fukunaga, Kazutoshi Miyashita, Kwijun Park, Naofumi Oyamada, Naoya Sawada, Daisuke Taura, Naohisa Tamura, Yasushi Kondo, Shinji Nito, Hirofumi Suemori, Norio Nakatsuji, Shin-Ichi Nishikawa, Kazuwa Nakao

Objective—We demonstrated previously that mouse embryonic stem (ES) cell–derived vascular endothelial growth factor receptor-2 (VEGF-*R2*)–positive cells can differentiate into both vascular endothelial cells and mural cells. This time, we investigated kinetics of differentiation of human ES cells to vascular cells and examined their potential as a source for vascular regeneration.

Methods and Results—Unlike mouse ES cells, undifferentiated human ES cells already expressed VEGF-*R2*, but after differentiation, a VEGF-*R2*-positive but tumor rejection antigen 1-60 (TRA1-60)–negative population emerged. These VEGF-*R2*-positive but tumor rejection antigen 1-60–negative cells were also positive for platelet-derived growth factor receptor α and β chains and could be effectively differentiated into both VE-cadherin$^+$ endothelial cell and α-smooth muscle actin$^+$ mural cell. VE-cadherin$^+$ cells, which were also CD34$^+$ and VEGF-*R2*$^+$ and thought to be endothelial cells in the early differentiation stage, could be expanded while maintaining their maturity. Their transplantation to the hindlimb ischemia model of immunodeficient mice contributed to the construction of new blood vessels and improved blood flow.

Conclusions—We could identify the differentiation process from human ES cells to vascular cell components and demonstrate that expansion and transplantation of vascular cells at the appropriate differentiation stage may constitute a novel strategy for vascular regenerative medicine. (***Arterioscler Thromb Vasc Biol.* 2007;27:2127-2134.**)

Key Words: angiogenesis ■ developmental biology ■ embryonic stem cells ■ vascular biology ■ endothelium

Pluripotent embryonic stem (ES) cells are gaining attention as promising cell sources for regenerative medicine, especially after the establishment of human ES cells.[1] Because the knockout animal research approach is not applicable to humans, investigating human cell development/differentiation using human ES cells is more helpful. These cells possess a number of characteristics distinct from those of mouse ES cells, such as surface antigens, leukemia inhibitory factor independency, and long doubling time.[1] We demonstrated previously that mouse ES cell–derived vascular endothelial growth factor (VEGF) receptor-2 (VEGF-*R2*)–positive cells can differentiate into both vascular endothelial cells (ECs) and mural cells (MCs), the latter composed of pericytes and vascular smooth muscle cells. We termed these mouse VEGF-*R2*$^+$ cells "vascular progenitor cells" (VPCs).[2] We also showed that VEGF and the vasodilating peptide adrenomedullin, which, as we reported previously, enhances angiogenesis,[3] play important roles in EC differentiation from these mouse VEGF-*R2*$^+$ cells.[4] However, recent studies have shown that, in undifferentiated human ES cells, unlike in mouse ES cells, VEGF-*R2* is expressed and continues to be expressed during differentiation associated with embryoid body formation.[5,6] To further clarify the vascular differentiation process in human beings and to determine the possible clinical application of ES cells to vascular regeneration, investigation of human ES cells is essential. It was also found that CD31$^+$ cells could be isolated from human embryoid bodies, indicating that they can act as ECs.[6] However, a precise analysis of the differentiation process

Original received February 27, 2007; final version accepted June 9, 2007.

From the Department of Medicine and Clinical Science (M.S., H.I., K.Y., T.Y-K., A.N., T-H.C., Naok.S., Y.F., K.M., K.P., N.O., Naoy.S., D.T., N.T., K.N.), Kyoto University Graduate School of Medicine, Kyoto, Japan; Department of Internal Medicine (H.I.), Keio University School of Medicine, Tokyo, Japan; Laboratory of Stem Cell Differentiation (J.K.Y.) and Laboratory of Embryonic Stem Cell Research (H.S.), Stem Cell Research Center, and Department of Development and Differentiation (N.N.), Institute for Frontier Medical Sciences, Kyoto University, Kyoto, Japan; Discovery Research Laboratory (Y.S., Y.K., S.N.), Tanabe Seiyaku Co, Ltd, Osaka, Japan; Center for Developmental Biology (S-I.N.), RIKEN, Kobe, Japan.

Correspondence to Hiroshi Itoh, Department of Medicine and Clinical Science, Kyoto University Graduate School of Medicine, 54 Shogoin Kawahara-cho, Sakyo-ku, Kyoto 606-8507, Japan. E-mail hiito@kuhp.kyoto-u.ac.jp

Arterioscler Thromb Vasc Biol. is available at http://atvb.ahajournals.org DOI: 10.1161/ATVBAHA.107.143149

from human ES cells to EC or other vascular cell components, such as MC, in the embryoid body differentiation system has so far not been possible.

In the study reported here, we identified the differentiation kinetics of human ES cells to vascular cell components by using our in vitro 2D differentiation system. Furthermore, we succeeded in establishing new human cell sources derived from human ES cells, which may be used for therapeutically effective transplantation in vivo.

Methods

Cell Culture

ES cells were maintained as described.[1,7] OP9 feeder cell lines were established and maintained as described,[8] whereas their growth was inactivated by mitomycin C.

To induce differentiation, ES cells were dissociated into small colonies with the aid of 0.1% collagenase (Wako) and cultured on an OP9 feeder layer in a differentiation medium (minimal essential medium, GIBCO) supplemented with 5×10^{-5} M 2-mercaptoethanol with 10% FCS. Sorted cells were recultured on a collagen IV–coated dish in the differentiation medium with the addition of 10% FCS, VEGF (100 ng/mL; PeproTech EC Ltd), or platelet-derived growth factor (PDGF)-BB (10 ng/mL) (PeproTech EC Ltd).

Flow Cytometry and Cell Sorting

Cells were detached by cell dissociation buffer (GIBCO) with or without collagenase and labeled with various fluorescence-conjugated monoclonal antibodies (please see http://atvb.ahajournals.org). Flow cytometry analysis and cell sorting were performed as described.[2,4,8]

Immunohistochemistry

Cultured cells were stained with various monoclonal antibodies (please see http://atvb.ahajournals.org) as described.[2,4] The immunofluorescence photographs were taken with a confocal laser-scanning microscope (LSM5-Pascal, Carl Zeiss).

Hindlimb Ischemia Model

Eight-week–old KSN/Slc and BALB/c Slc nude mice were purchased from SLC Japan. After anesthetization with pentobarbital (80 mg/kg IP), the right femoral vein was ligated. We injected 5×10^5 cells in 100 μL of PBS or 100 μL of PBS only into the right femoral artery. Immediately after the cell injection, the right femoral artery was ligated and excised.[9] Experimental procedures were performed in accordance with Kyoto University standards for animal care. Hindlimb blood flow was measured with a laser Doppler perfusion image analyzer (Moor Instruments Ltd), as described.[9] Biotin-conjugated Griffonia simplicifolia lectin I-isolectin B_4 (Vector Laboratories) was injected into the portal vein 15 minutes before sacrifice. After fixation with 4% paraformaldehyde, the ischemic lower legs were embedded in optimal cutting temperature compound (Sakura Finetechnical Co Ltd) and frozen. Capillary numbers were examined by counting the number of capillaries stained with anti-human and/or mouse CD31 antibody. Ten random fields on 2 different sections (≈3 mm apart) from each mouse were photographed and analyzed by National Institutes of Health imaging as described.[9] The vessel area and length were measured quantitatively with the Kurabo angiogenesis image analyzer (Kurabo).

Teratoma Formation Study

We transplanted 5×10^5 cells in 50 μL of PBS under the dorsal back skin of SCID mice (CLEA Japan, Inc), which are commonly used for teratoma formation for human ES cells.[1,7] After 5 months, 1 cm^2 of the skin around the point of injection was harvested, and the excised tissue was serially sectioned (10 μm) at 200-μm intervals.

Analysis of Angiogenic Factor mRNA Expression

Total cellular RNA was isolated from VPCs or ECs in the early differentiation stage (eECs) with RNAeasy Mini kit (Qiagen KK). The mRNA expression was analyzed with the One-Step RNA PCR kit (TaKaRa). Primer pairs were purchased from R&D Systems Inc. PCRs were performed as manufacturers protocols.

Measurement of Angiogenic Factors in VPC- or eEC-Conditioned Media

Cells (1×10^6) of VPCs or eECs were plated on 10-cm dishes and incubated with 5 mL of media (minimal essential medium with 0.5% bovine serum) for 72 hours. The concentrations of human VEGF, basic fibroblast growth factor (bFGF), and hepatocyte growth factor (HGF) were measured by SRL, Inc. Human PDGF-BB was measured with the Human PDGF-BB Quantikine ELISA kit (R&D Systems Inc).

Statistical Analysis

Results are presented as mean±SEM. In the hindlimb ischemia model, the statistical significance was evaluated using ANOVA followed by Fisher's analysis for comparisons between 2 means. $P<0.05$ was considered significant.

Results

Differentiation Pathway of Human ES Cells to Vascular Cell Components

First, we examined the expression of VEGF-*R*2 and some putative stem cell markers on a human ES cell line, HES3, which was established at Monash University in Australia.[1] Approximately 50% of undifferentiated human ES cells expressed VEGF-*R*2, whereas these cells were also positive for AC133 and c-Kit but negative for CD34, respectively (Figure 1A). We also analyzed the expression of tumor rejection antigen (TRA) 1-60 on these human ES cells. The TRA1 antigen is expressed on the surface of human tetracarcinoma stem cells, human embryonic germ cells, and human ES cells. Thus, we used it as a marker of the human ES cell. The VEGF-$R2^+$ population of human ES cells was also positive for TRA1-60 (Figure 1B).

Next, we induced differentiation of human ES cells in an in vitro 2D culture on an OP9 stromal cell line. Although monkey ES cells have effectively differentiated as single cells on an OP9 layer,[10] human ES cells have not survived as single cells. We, therefore, plated small human ES cell colonies on OP9 to induce differentiation. Under these conditions, the TRA1-60^+ cell population gradually decreased in number during differentiation. On the other hand, a VEGF-$R2^+$ TRA1-60^- population emerged and accounted for ≈15% of all of the cells on day 8 (Figure 1C). We confirmed the differentiation kinetics of human ES cells by using another human ES cell line, KhES-1, established by us.[7] Similar to the HES3 cell line, VEGF-*R*2 was low positive, and the VEGF-$R2^+$ cells were also TRA1-60^+ in undifferentiated KhES-1 (Figure 1D). After differentiation on an OP9 feeder layer, VEGF-$R2^+$ TRA1-60^+ cells decreased, and VEGF-$R2^+$ TRA1-60^- cells appeared on days 8 (Figure 1E). Next, we analyzed the expression of several cell surface markers on the VEGF-$R2^+$ TRA1-60^- population on day 8 of HES3. Flt1 was positive, c-Kit and CXCR4 were both negative, PDGR receptor (PDGFR)α and PDGFRβ were positive, AC133

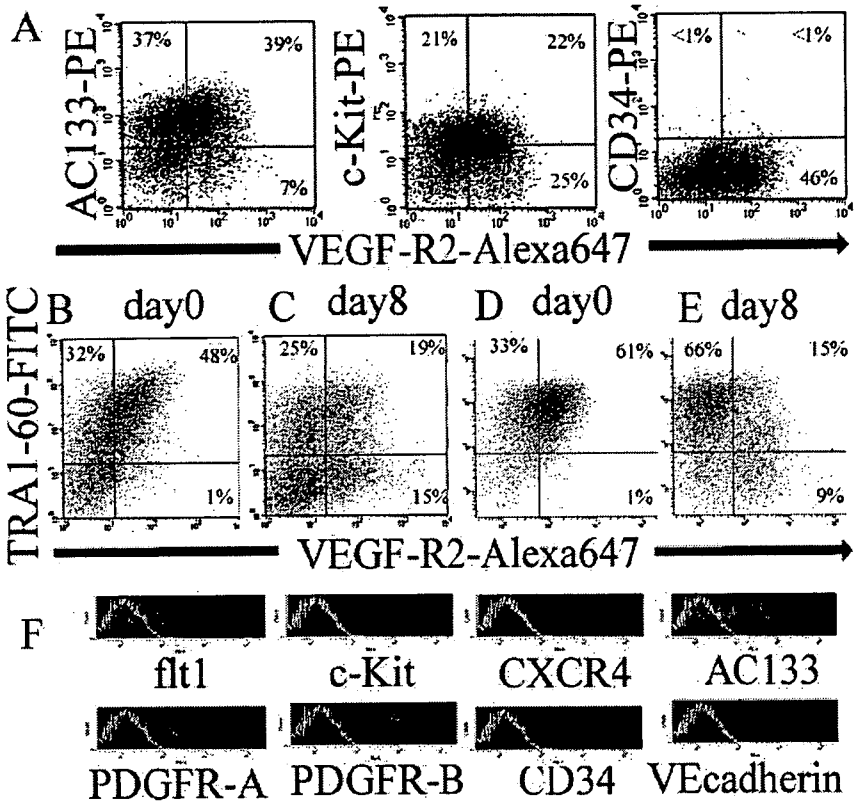

Figure 1. Flow cytometry analysis of differentiation kinetics of human ES cells. A, Expression of cell surface markers on undifferentiated human ES cells (HES3). B through E, TRA1-60 and VEGF-*R2* expression on 2 human ES cell lines (HES3 and KhES-1) during differentiation on an OP9 feeder layer. B and C, HES3; D and E, KhES-1. F, Cell surface marker expression on VEGF-*R2*$^+$ TRA1-60$^-$ cells on day 8.

was still positive, and CD34 and vascular endothelial cadherin (VE-cadherin) were negative on a large population of the VEGF-*R2*$^+$ TRA1-60$^-$ cells (Figure 1F). Monocyte markers, such as CD45, Cd11b, and CD14, were negative.

The VEGF-*R2*$^+$ TRA1-60$^-$ and VE-cadherin–negative cells were sorted by flow cytometry on day 8 and cultured on a collagen IV–coated dish without a feeder cell layer for an additional 8 days in the presence of 10% FCS and VEGF. This cell culturing condition induced the emergence of CD34$^+$, VE-cadherin$^+$, CD31$^+$, and endothelial NO synthase–positive cells (Figure 2A through 2D), which can be categorized as ECs. The rest of the cells negative for CD31 were polygonal in shape and showed α-smooth

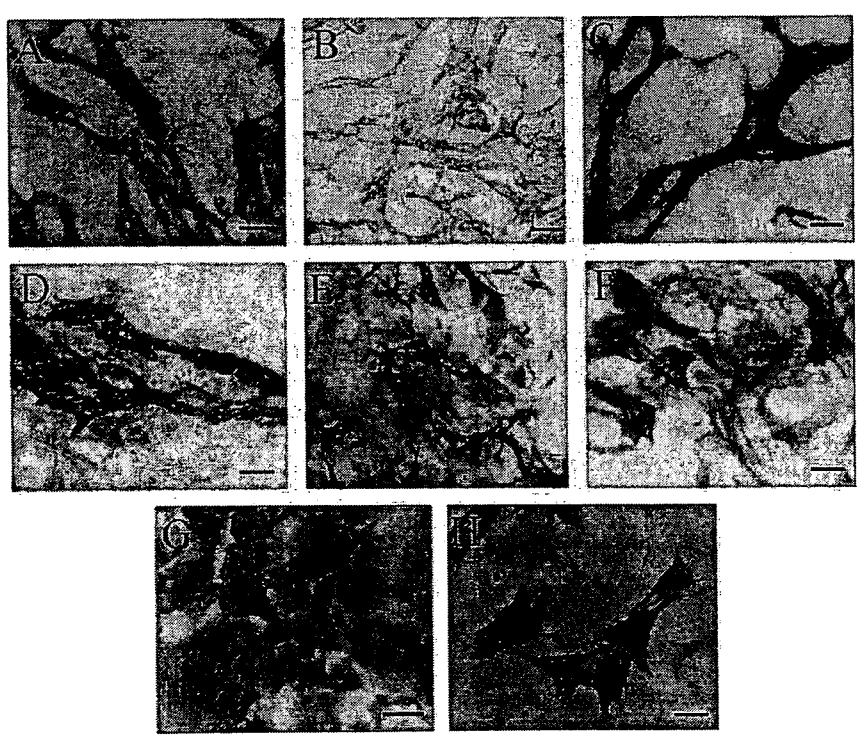

Figure 2. Immunocytological analysis of differentiation of vascular progenitor cells into vascular cells. A through D, Immunostaining for endothelial cell markers on VEGF-*R2*$^+$ TRA1-60$^-$ cells recultured with VEGF and FBS. A, CD34; B, VE-cadherin; C, CD31; D, endothelial NO synthase; E, Double immunostaining for CD31 (blue) and α-smooth muscle actin (brown). F and G, Immunostaining for MC markers on VEGF-*R2*$^+$TRA1-60$^-$ cells recultured with FBS. F, α-Smooth muscle actin; G, Calponin; H, Immunostaining for α-smooth muscle actin with treatment of PDGF-BB on VEGF-*R2*$^+$ TRA1-60$^-$ cells. Scale bars, 50 μm.

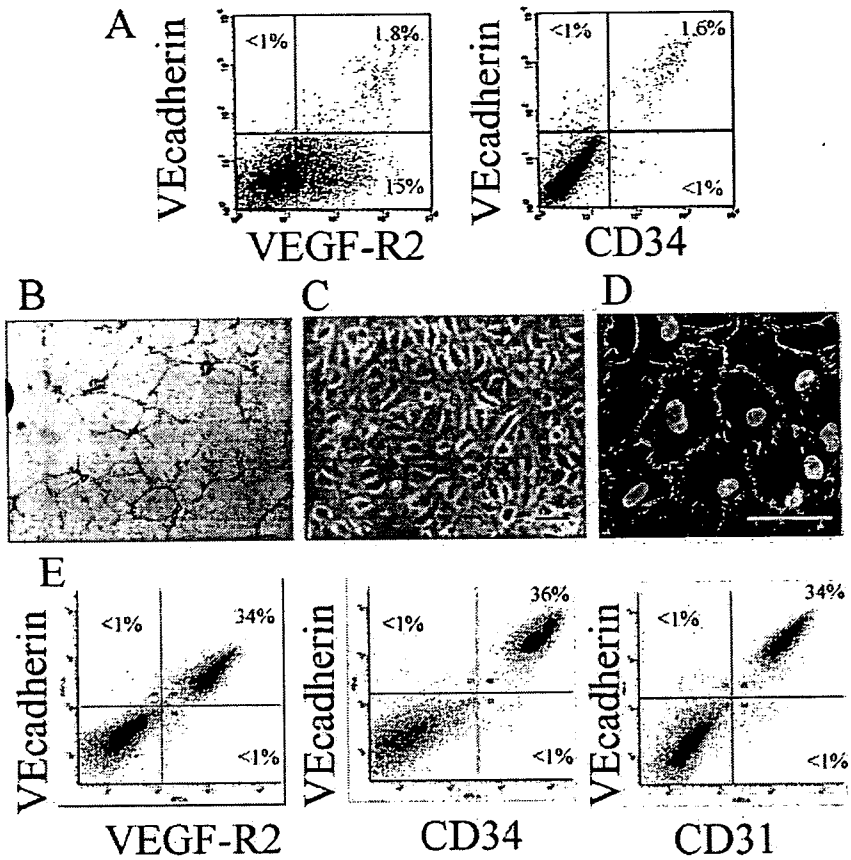

Figure 3. Isolation and expansion of vascular eECs. A, Flow-cytometric analysis of human ES cell–derived cells on an OP9 feeder layer on day 10. B, Network formation of human ES cell–derived VE-cadherin$^+$ cells (eECs) after 24-hour culture on Matrigel. C, Phase-contrast microscopic analysis of recultured VE-cadherin$^+$ cells on a collagen IV–coated dish. D, Immunostaining of recultured VE-cadherin$^+$ cells; red, CD31; green, nuclear staining (SYBR-Green I). E, Flow-cytometric analysis of the cells at the sixth passage expanded from VE-cadherin$^+$ cells. Scale bar, 50 μm.

muscle actin expression (Figure 2E). In the absence of VEGF, VEGF-$R2^+$ TRA1-60$^-$ cells did not differentiate into ECs, but almost all of them differentiated into α-smooth muscle actin and calponin-positive cells, which can be categorized as MCs (Figure 2F and 2G). Because these VEGF-$R2^+$ TRA1-60$^-$ cells expressed PDGFRβ, PDGF-BB with 0.5% FCS induced MC induction in a similar manner (Figure 2H). We, therefore, concluded that these VEGF-$R2^+$ TRA1-60$^-$ cells could be categorized as human VPCs that can differentiate into both ECs and MCs. Next we examined whether VEGF-$R2^+$ TRA1-60$^+$ cells after 8 days of differentiation is immature or not. Before differentiation, VEGF-$R2^+$ TRA1-60$^+$ cells were positive for flt1, AC133, and c-Kit and negative for CXCR4, PDGFRα, PDGFRβ, CD34, and VE-cadherin. However, after 8 days of differentiation, c-Kit expression decreased, and PDGFRα-positive and/or β-positive cells appeared in VEGF-$R2^+$ TRA1-60$^+$ cells (data not shown). Thus, VEGF-$R2^+$ TRA1-60$^+$ cells after 8 days of differentiation were not equivalent to the immature ES cells on day 0.

Isolation and Expansion of Vascular eECs

Next, we focused our attention on VE-cadherin$^+$ ECs that were more differentiated than the VPC. On 10 days of differentiation of HES3 on an OP9 feeder layer, VEGF-$R2^+$ and VE-cadherin$^+$ cells emerged and accounted for $\approx$1% to 2% of all the cells (Figure 3A). This VE-cadherin–positive cell population was almost identical to the CD34$^+$ population (Figure 3A). We sorted these VE-cadherin$^+$ cells, and, because these cells were also VEGF-$R2^+$ and CD34$^+$ (Figure 3A), we used the term "eEC" for these EC in the early differentiation stage. These cells formed a network-like structure on Matrigel in vitro (Figure 3B), showed a cobblestone appearance when they became confluent (Figure 3C), and immunofluorescence staining with CD31 showed a characteristic marginal staining pattern (Figure 3D). These eECs were negative for monocyte makers CD45, CD11b, and CD14 (data not shown) and could be successfully propagated by a factor of $\approx 1.2\times10^2$ (from 2×10^5 cells to 2.4×10^7 cells) after 6 passages on collagen IV–coated dishes. They were cultured with a cell density of 1.5×10^4 cells/cm^2 with VEGF because they did not expand when they were more sparsely plated or cultured without VEGF. Flow-cytometric analysis showed that VE-cadherin$^+$ cells were reduced to $\approx$35% of the total number of cells after 6 passages (Figure 3E), but they were still VEGF-$R2^+$, CD34$^+$, and CD31$^+$ at the sixth passage, indicating that the cell differentiation stage had been maintained (Figure 3E). In another series of experiments, we sorted these VE-cadherin$^+$ cells on day 10 and replated them on an OP9 feeder layer or nonfeeder collagen IV–coated dishes for 1 additional week. The VE-cadherin$^+$ cells in these 2 culture groups were then resorted and plated on nonfeeder collagen IV–coated dishes for reculturing. After an additional 3 weeks of reculturing, VE-cadherin expression was examined. The cells that were cultured for 1 additional week on OP9 were 90% positive for VE-cadherin, but the cells kept on nonfeeder dishes were only 44% positive. This suggests that VE-cadherin$^+$ eECs still retain the potential to differentiate

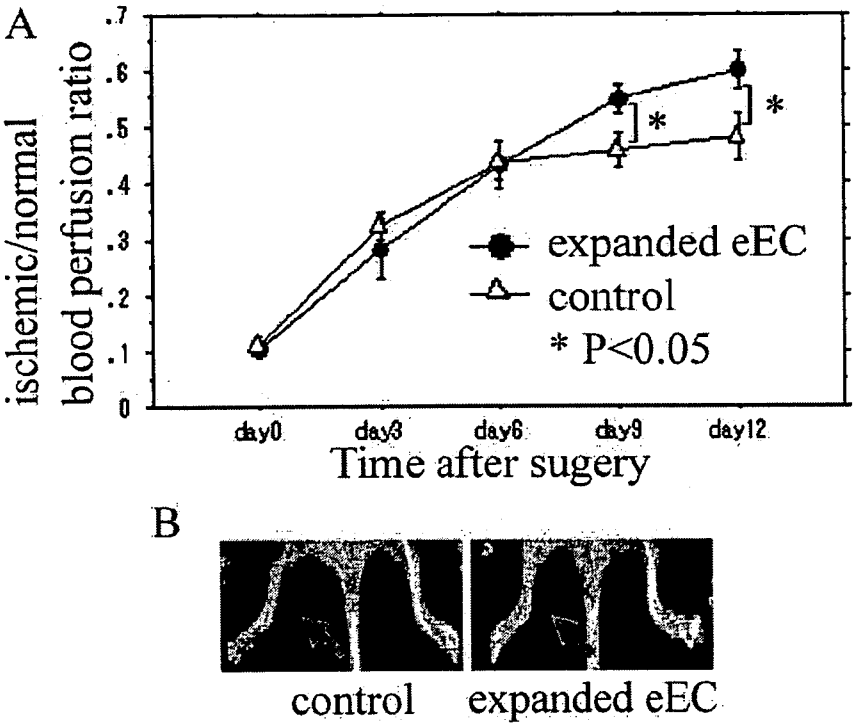

Figure 4. Transplantation of human ES cell–derived vascular cells to the hindlimb ischemia model of immunodeficient mice. A, Quantitative analysis of the hindlimb blood flow by means of calculating the ischemic/normal limb perfusion ratios in mice with ischemic hindlimb. *$P<0.05$. On days 9 and 12, the blood flow in the ischemic limb of the expanded eEC-injected mice (n=8) had increased significantly compared with that of control mice (n=8). B, Representative laser Doppler perfusion images on day 12.

into other cell types, but more differentiated VE-cadherin$^+$ ECs may lose this ability.

Transplantation of Human ES Cell-Derived Vascular Cells to the Hindlimb Ischemia Model of Immunodeficient Mice

As the next step, we investigated whether human ES cell–derived vascular cells can be used for vascular regeneration in cell transplantation in the hindlimb ischemia model. KSN nude mice received an intra-arterial injection of cells in PBS or PBS only into the right femoral artery, followed by right femoral artery ligation and removal to create hindlimb ischemia. VEGF-$R2^+$ TRA1-60$^-$ cells, identified as VPCs, were transplanted, but laser Doppler perfusion image analysis on day 14 showed no significant difference in recovery of the blood flow (expressed as the ischemic/normal limb blood perfusion ratio) between the cell-transplanted mice (0.496 ± 0.29; n=10) and the control PBS-injected mice (0.433 ± 0.42; n=14). Next, we used the eECs expanded at passages 4 to 6. As shown in Figure 4A and 4B, the hindlimb blood flows had significantly improved in the cell-injected group 9 and 12 days after injection. For histological analysis, transplanted cells had been labeled with CM-DiI before cell transplantation, and biotin-conjugated isolectin B_4 was intravenously injected to stain ECs before sacrifice on day 14. Although some of the transplanted cells were incorporated as isolectin B4$^+$ vascular ECs in the large vessels (Figure 5A), most of the transplanted cells were incorporated as small capillaries (Figure 5B). To quantify the capillary density, sections of the ischemic hindlimbs were stained with anti-mouse and human-specific CD31 antibodies (Figure 5C and 5D). Human CD31$^+$ capillaries were detected in the expanded eEC-transplanted mice. The mouse and/or human CD31$^+$ total capillary number and area significantly increased in the expanded eEC-transplanted group compared with the control PBS-injected group, whereas there was tendency but no significant difference in the mouse CD31$^+$ host capillary number and area (Figure 5E and 5F). On the other hand, there was no significant difference in the capillary length (Figure 5G). Because we cut our sections at right angles with muscle fibers and femoral artery, it might be difficult to estimate the capillary density by vessel length.

Next we performed our transplantation experiments with the same procedure using BALB/c Slc nude mice, in which hindlimb ischemia is more severe than in KSN/Slc nude mice. PBS, VPCs, eECs or human adult aortic ECs were transplanted, and the ischemic hindlimbs were observed on day 14. In the PBS-injected mice, the ischemic hindlimb was autoamputated in 3 of 7 mice, and mild necrosis was observed in 1 of 7. In the VPC-transplanted mice, 3 of 7 were autoamputated and mild necrosis was seen in 2 of 7. In the eEC-transplanted mice, the ischemic hindlimb was not autoamputated, and only mild necrosis was observed in 2 of 8. In the human adult aortic EC-transplanted mice, 4 of 7 were auto-amputated, and mild necrosis was seen in 1 of 7. Furthermore, sections of the ischemic hindlimb in mice without autoamputation were stained with anti-mouse and human-specific CD31 antibodies. Human CD31$^+$ capillaries were most abundant in the eEC-transplanted mice, although some human CD31$^+$ cells were detected in the VPC or human adult aortic EC-transplanted mice (please see http://atvb.ahajournals.org).

Exclusion of Possible Teratoma Formation by the Expanded eEC

Further experiments were conducted to detect possible teratoma formation by eEC. We conducted long-term follow-ups

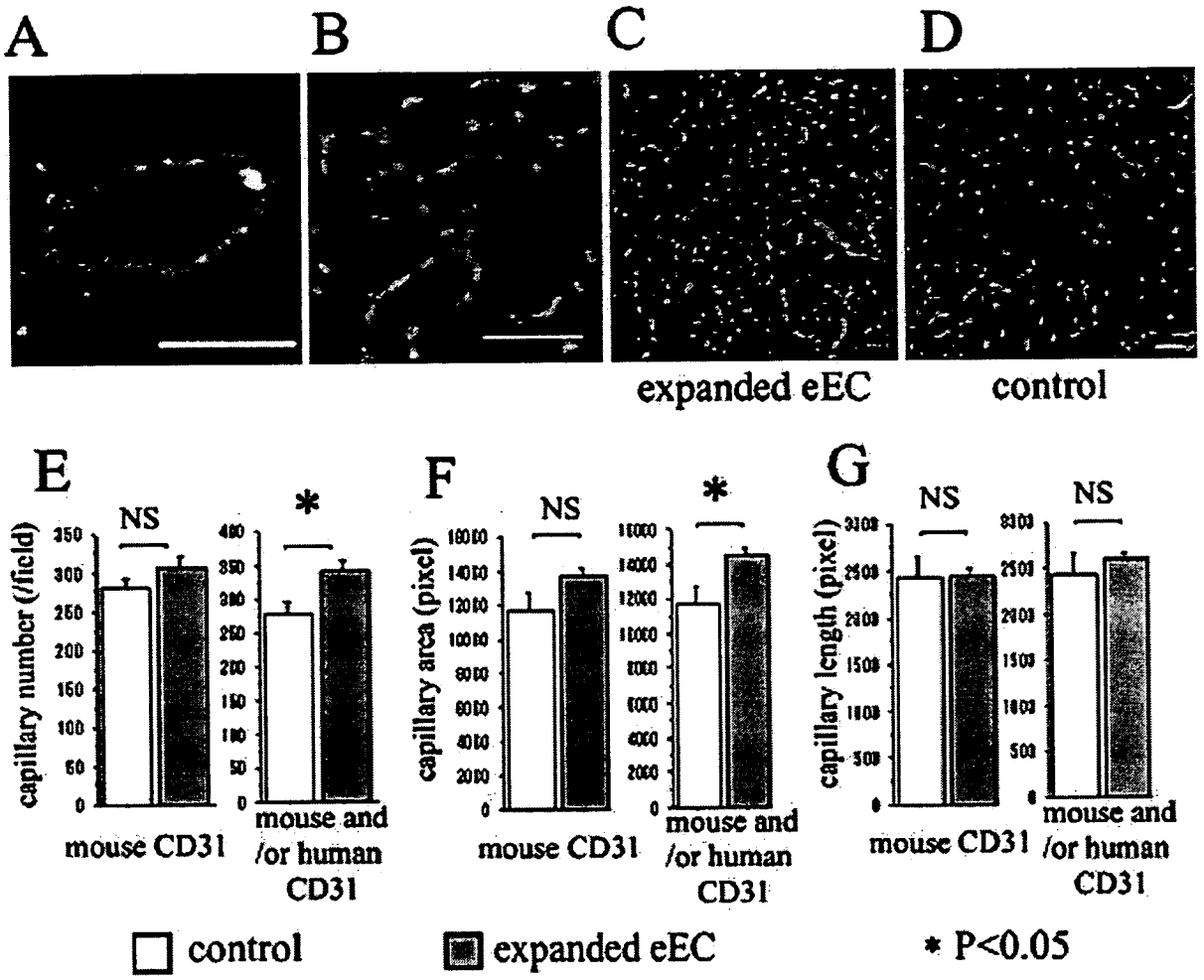

Figure 5. A and B, Histological analysis of vascular regeneration by the intra-arterially injected expanded eEC; green, isolectin B_4^+ endothelial cells; red, CM-DiI$^+$ transplanted cells (representative photographs). C and D, Fluorescent photographs of ischemic hindlimb for capillary density analysis; green, mouse CD31$^+$ capillaries; red, human CD31$^+$ capillaries (representative photographs). E through G, Quantitative analysis of the mouse and human endothelial cell marker–positive capillary densities in the ischemic hindlimb. E, capillary numbers. F, capillary areas. G, capillary lengths. Scale bars, 50 μm.

by transplanting expanded eECs or undifferentiated human ES cells into 3 mice each and following them for 5 months. We transplanted 5×10^5 cells under the dorsal back skin of SCID mice, which are commonly used for teratoma formation for human ES cells. Large tumors had formed after 3 to 5 months in 2 of the 3 mice in the human ES cell–transplanted group, but none had formed in any of the 3 mice in the expanded eEC-transplanted group. In immunohistological analysis, HLA-ABC$^+$ tumors were not observed in the subcutaneous region of eEC transplanted mice, although only a few HLA-ABC$^+$ human cells were remaining (data not shown).

Expression of Angiogenic Factors in Human ES Cell–Derived Vascular Cells

In addition, we investigated whether VPC or eEC produced major angiogenic factors such as VEGF, bFGF, human growth factor, and PDGF-BB. RT-PCR analysis detected mRNA expressions of VEGF, bFGF, and human growth factor in VPCs and PDGF-B and bFGF in eECs (please see http://atvb.ahajournals.org). We measured the protein concentration of these angiogenic factors in culture media by ELISA; however, the concentration of VEGF, human growth factor, and PDGF-BB did not reached the detectable level, and the concentration of bFGF was <30 pg/mL.

Discussion

In this study, we were able to clarify the differentiation process from human ES cells to mature vascular cell components. In adults, VEGF and PDGF receptors are expressed on EC and MC, respectively, and VEGF and PDGF stimulate the growth of the respective cell types. In this study, human ES cell–derived VPCs expressed both VEGF and PDGF receptors. In addition, stimulation with VEGF and PDGF-BB induced 2 differentiation pathways for EC and MC in this cell population. In mouse embryos, VEGF-*R*2 and PDGFRα were reported to be expressed in the mesoderm.[11] In whole-mount immunohistochemistry of mouse embryos (E7.5 to 8), VEGF-*R*2 was expressed predominantly in the extraembryonic and proximal-lateral mesoderm. PDGFRα was detected mainly in the paraxial embryonic mesoderm. Both VEGF-*R*2 and PDGFRα were

detected in the anterior paraxial mesoderm. It was also reported that vascular endothelial precursors were identified from the cephalic mesoderm of the avian embryo labeled using an antibody against Quek1 (avian homolog of VEGF-*R*2).[12] Our result that VEGF-*R*2$^+$ PDGFR$^+$ VPCs can differentiate into vascular cells may agree with their reports. In our transplantation examination, some human CD31$^+$ ECs were observed in the ischemic hindlimb of VPC-transplanted mice. This suggests that some transplanted VPC (negative for CD31) differentiated into CD31$^+$ ECs in vivo.

In addition, we investigated whether human ES cell–derived vascular cells can be used for vascular regeneration. Transplanted eECs were successfully incorporated into the host circulation and significantly accelerated improvement of local blood flow, whereas VPCs did not. We reported recently that VEGF-*R*2$^+$ cells derived from mouse ES cells could differentiate into not only vascular cells but also cardiomyocytes.[13] Thus, VPCs may be too immature to be used directly as the source for vascular regeneration. It has also been reported that ischemia-induced neovascularization did not improve in mice receiving human mature ECs (eg, human microvascular ECs).[14] Their report is compatible with our result that human adult aortic EC transplantation had no effect for the prevention of ischemic necrosis. The induction and isolation of the cells at the differentiation stage most appropriate for transplantation seem to be important. Judging from our results obtained from histological analysis and capillary density evaluation, at least some of the therapeutic effect of transplantation of expanded eECs could be attributed to vascular regeneration as a result of incorporation of the transplanted cells into the host vessels. Because RT-PCR analysis detected mRNA expression of PDGF-B not in VPCs but in eECs, PDGF-BB secretion might affect the effect of eEC transplantation, although PDGF-BB did not reached the detectable level in culture media. In adults, endothelial progenitor cells (EPCs) reportedly participate in postnatal angiogenesis,[15] whereas other reports suggest that EPCs contribute to neovascularization in tissue ischemia.[14] However, the expansion of EPCs in sufficient quantities to improve blood flow in large animals has not yet been achieved. In addition, some recent reports suggest that adult bone marrow–derived cells, such as EPCs, do not transdifferentiate into ECs under physiological conditions.[16,17] Although the role of EPCs as a modifier of vascular growth awaits further investigation, our findings may help provide an alternative and novel supply of vascular cells for cell therapy as a contribution to vascular regenerative medicine.

Furthermore, the establishment of an in vitro differentiation system of human vascular cell components from human ES cells in this study should also make it possible to dissect out cellular mechanisms in human vascular development and diseased states for which the knockout animal research approach is not practical. Trials on gene expression profiling using our in vitro differentiation system of human vascular cells from human ES cells could assist in the search for novel gene products to develop new therapeutic approaches for vascular regeneration.

Acknowledgments

The human ES cells (HES-3) were contributed by ES Cell International Pte Ltd, Singapore. The anti-human VEGF-*R*2 antibody (KM1668) was a generous gift from M. Shibuya, MD, PhD, Department of Cancer Biology, Institute of Medical Science, University of Tokyo.

Sources of Funding

This work was supported by Grants-in-Aid for Scientific Research from the Ministry of Health, Labour and Welfare and the Ministry of Education, Culture, Sports, Science and Technology. This work was also supported by a grant from the Japan Smoking Foundation, a Japan Heart Foundation/Pfizer Japan Grant for Cardiovascular Disease Research, and a grant from the Study Group for Molecular Cardiology Research. This work was also supported by Fellowships of the Japan Society for the Promotion of Young Scientists and Establishment of International COE for Integration of Transplantation Therapy and Regenerative Medicine (COE program of the Ministry of Education, Culture, Sports, Science and Technology, Japan).

Disclosures

None.

References

1. Reubinoff BE, Pera MF, Fong CY, Trounson A, Bongso A. Embryonic stem cell lines from human blastocysts: somatic differentiation in vitro. *Nature Biotechnology.* 2000;18:399–404.
2. Yamashita J, Itoh H, Hirashima M, Ogawa M, Nishikawa S, Yurugi T, Naito M, Nakao K, Nishikawa S. Flk1-positive cells derived from embryonic stem cells serve as vascular progenitors. *Nature.* 2000;408:92–96.
3. Miyashita K, Itoh H, Sawada N, Fukunaga Y, Sone M, Yamahara K, Yurugi-Kobayashi T, Park K, Nakao K. Adrenomedullin provokes endothelial Akt activation and promotes vascular regeneration both in vitro and in vivo. *FEBS Lett.* 2003;544:86–92.
4. Yurugi-Kobayashi T, Itoh H, Schroeder T, Nakano A, Narazaki G, Kita F, Yanagi K, Hiraoka-Kanie M, Inoue E, Ara T, Nagasawa T, Just U, Nakao K, Nishikawa, SI. Yamashita, JK. Adrenomedullin/cyclic amp pathway induces notch activation and differentiation of arterial endothelial cells from vascular progenitors. *Arterioscler Thromb Vasc Biol.* 2006;26:1977–1984.
5. Kaufman DS, Hanson ET, Lewis RL, Auerbach R, and Thomson JA. Hematopoietic colony-forming cells derived from human embryonic stem cells. *Proc Natl Acad Sci U S A.* 2001;98:10716–10721.
6. Levenberg S, Golub JS, Amit M, Itskovitz-Eldor J, Langer R. Endothelial cells derived from human embryonic stem cells. *Proc Natl Acad Sci U S A.* 2002;99:4391–4396.
7. Fujioka T, Yasuchika K, Nakamura Y, Nakatsuji N, Suemori H. A simple and efficient cryopreservation method for primate embryonic stem cells. *Int J Dev Biol.* 2004;48:1149–1154.
8. Hirashima M, Kataoka H, Nishikawa S, Matsuyoshi N, Nishikawa S. Maturation of embryonic stem cells into endothelial cells in an in vitro model of vasculogenesis. *Blood.* 1999;93:1253–1263.
9. Yamahara K, Itoh H, Chun TH, Ogawa Y, Yamashita J, Sawada N, Fukunaga Y, Sone M, Yurugi-Kobayashi T, Miyashita K, Tsujimoto H, Kook H, Feil R, Garbers DL, Hofmann F, Nakao K. Significance and therapeutic potential of the natriuretic peptides/cGMP/cGMP-dependent protein kinase pathway in vascular regeneration. *Proc Natl Acad Sci U S A.* 2003;100:3404–3409.
10. Sone M, Itoh H, Yamashita J, Yurugi-Kobayashi T, Suzuki Y, Kondo Y, Nonoguchi A, Sawada N, Yamahara K, Miyashita K, Park K, Shibuya M, Nito S, Nishikawa S, Nakao K. Different differentiation kinetics of vascular progenitor cells in primate and mouse embryonic stem cells. *Circulation.* 2003;107:2085–2088.
11. Kataoka H, Takakura N, Nishikawa S, Tsuchida K, Kodama H, Kunisada T, Risau W, Kita T, Nishikawa SI. Expressions of PDGF receptor alpha, c-Kit and Flk1 genes clustering in mouse chromosome 5 define distinct

subsets of nascent mesodermal cells. *Dev Growth Differ.* 1997;39: 729–740.
12. Couly G, Coltey P, Eichmann A, Le Douarin NM. The angiogenic potentials of the cephalic mesoderm and the origin of brain and head blood vessels. *Mech Dev.* 1995;53:97–112.
13. Yamashita JK, Takano M, Hiraoka-Kanie M, Shimazu C, Peishi Y, Yanagi K, Nakano A, Inoue E, Kita F, Nishikawa S. Prospective identification of cardiac progenitors by a novel single cell-based cardiomyocyte induction. *FASEB J.* 2005;19:1534–1536.
14. Kalka C, Masuda H, Takahashi T, Kalka-Moll WM, Silver M, Kearney M, Li T, Isner JM, Asahara T. Transplantation of ex vivo expanded endothelial progenitor cells for therapeutic neovascularization. *Proc Natl Acad Sci U S A.* 2000;97:3422–3427.
15. Asahara T, Murohara T, Sullivan A, Silver M, van der Zee R, Li T, Witzenbichler B, Schatteman G, Isner JM. Isolation of putative progenitor endothelial cells for angiogenesis. *Science.* 1997;275: 964–967.
16. O'Neill TJ 4th, Wamhoff BR, Owens GK, Skalak TC. Mobilization of bone marrow-derived cells enhances the angiogenic response to hypoxia without transdifferentiation into endothelial cells. *Circ Res.* 2005;97: 1027–1035.
17. Zentilin L, Tafuro S, Zacchigna S, Arsic N, Pattarini L, Sinigaglia M, Giacca M. Bone marrow mononuclear cells are recruited to the sites of VEGF-induced neovascularization but are not incorporated into the newly formed vessels. *Blood.* 2006;107:3546–3554.

Am J Physiol Endocrinol Metab 293: E819–E825, 2007.
First published June 26, 2007; doi:10.1152/ajpendo.00681.2006.

Effects of ghrelin administration on decreased growth hormone status in obese animals

Hiroshi Iwakura,[1] Takashi Akamizu,[1] Hiroyuki Ariyasu,[1] Taiga Irako,[1] Kiminori Hosoda,[2] Kazuwa Nakao,[2] and Kenji Kangawa[1,3]

[1]*Ghrelin Research Project, Translational Research Center, Kyoto University Hospital;* [2]*Department of Medicine and Clinical Science, Endocrinology and Metabolism, Kyoto University Graduate School of Medicine, Kyoto; and* [3]*Department of Biochemistry, National Cardiovascular Center Research Institute, Osaka, Japan*

Submitted 13 December 2006; accepted in final form 22 June 2007

Iwakura H, Akamizu T, Ariyasu H, Irako T, Hosoda K, Nakao K, Kangawa K. Effects of ghrelin administration on decreased growth hormone status in obese animals. *Am J Physiol Endocrinol Metab* 293: E819–E825, 2007. First published June 26, 2007; doi:10.1152/ajpendo.00681.2006.—Obesity is characterized by markedly decreased ghrelin and growth hormone (GH) secretion. Ghrelin is a GH-stimulating, stomach-derived peptide that also has orexigenic action. Ghrelin supplement may restore decreased GH secretion in obesity, but it may worsen obesity by its orexigenic action. To reveal effects of ghrelin administration on obese animals, we first examined acute GH and orexigenic responses to ghrelin in three different obese and/or diabetic mouse models: *db/db* mice, mice on a high-fat diet (HFD mice), and Akita mice for comparison. GH responses to ghrelin were significantly suppressed in *db/db*, HFD, and Akita mice. Food intake of *db/db* and Akita mice were basally higher, and further stimulation of food intake by ghrelin was suppressed. Pituitary GH secretagogue receptor mRNA levels in *db/db* and HFD mice were significantly decreased, which may partly contribute to decreased GH response to ghrelin in these mice. In Akita mice for comparison, decreased hypothalamic GH-releasing hormone (GHRH) mRNA levels may be responsible for decreased GH response, since maximum GH response to ghrelin needs GHRH. When ghrelin was injected into HFD mice with GHRH coadministrated, GH responses to ghrelin were significantly emphasized. HFD mice injected with low-dose ghrelin and GHRH for 10 days did not show weight gain. These results indicate that low-dose ghrelin and GHRH treatment may restore decreased GH secretion in obesity without worsening obesity.

growth hormone secretagogue receptor; obesity; diabetes

IN HUMANS, OBESITY IS CHARACTERIZED by markedly decreased growth hormone (GH) production and secretion (3, 26). GH stimulates lipolysis and increases lean body mass, which may help to combat obesity. Decreased GH secretion in the context of obesity may promote additional fat deposition and promote weight gain (10). GH, however, does contribute to insulin resistance, which could worsen diabetes (7).

Ghrelin is a 28-amino acid peptide with unique acylation modification, which is essential for its biological action (14). Ghrelin was originally identified in the rat stomach as an endogenous ligand for an orphan receptor, which so far has been called GH secretagogue receptor (GHS-R) (14). Ghrelin is involved in a wide variety of functions, including regulation of GH release, gastric acid secretion, gastric motility, blood pressure, and cardiac output (4, 8, 18, 19, 23, 28). Ghrelin also has several metabolic functions, including orexigenic action (20, 22), reduction of insulin (5), and control of energy expenditure (24), which are all involved in the pathophysiology of adiposity or diabetes.

Plasma ghrelin level is suppressed in obesity (25), which may compensate for increased body weight by reducing its orexigenic activity, whereas low plasma ghrelin level may contribute to decreased GH secretion in obesity. Furthermore, Poykko et al. (21) reported that low plasma ghrelin level is associated with insulin resistance and incidence of type 2 diabetes.

To elucidate whether ghrelin supplementation can restore decreased GH secretion in obesity, we first determined acute GH and orexigenic responses to ghrelin in three different obese and/or diabetic mice models: *db/db* mice (a genetically obese mouse model with diabetes), mice on a high-fat diet (HFD; a diet-induced obese mouse model with moderate glucose intolerance), and Akita mice for comparison (an insulin-deprived diabetic nonobese mouse model) (29). Then, we determined how the ghrelin-GH system is modulated in the pituitaries and hypothalamuses of these animals. Last, we examined the effect of chronic ghrelin and GH-releasing hormone (GHRH) administration on diet-induced obesity.

MATERIALS AND METHODS

Experimental animals. Eight-week-old male *db/db* and control mice (misty) were purchased from CLEA Japan, (Tokyo, Japan). As a diet-induced model of obesity, 5-wk-old male C57BL/6J mice, purchased from Japan SLC (Shizuoka, Japan), were maintained on a HFD of 60% fat/kcal (Research Diets, New Brunswick, NJ) for 20 wk. Those maintained on a standard diet were used as control mice for HFD mice. Eight-week-old male Akita mice and C57BL/6J control mice were purchased from Japan SLC. Animals were maintained on standard rat food (CE-2, 352 kcal/100 g; CLEA Japan) with a 12:12-h light-dark cycle unless otherwise indicated. All experimental procedures were approved by the Kyoto University Graduate School of Medicine Committee on Animal Research.

Acute GH response to ghrelin and GHRH. Rat ghrelin (40, 120, and 360 μg/kg; Peptide Institute, Osaka, Japan), human GHRH (60 μg/kg; Mecasermin, Astellas Pharma, Tokyo, Japan), or saline was injected subcutaneously into mice on an ad libitum feeding schedule. Blood was collected from retroorbital veins 15 or 30 min after injection. Serum was isolated by centrifugation and stored at −20°C until assayed.

Measurements of hormones and free fatty acid levels. Serum GH levels were determined by rat growth hormone EIA kit (SPI bio,

Address for reprint requests and other correspondence: H. Iwakura, Ghrelin Research Project, Translational Research Center, Kyoto University Hospital, 54 Shogoin Kawahara-cho, Sakyo-ku, Kyoto 606-8507, Japan (e-mail: hiwaku@kuhp.kyoto-u.ac.jp).

The costs of publication of this article were defrayed in part by the payment of page charges. The article must therefore be hereby marked "*advertisement*" in accordance with 18 U.S.C. Section 1734 solely to indicate this fact.

Table 1. *Basal profiles of db/db mice on HFD and Akita mice*

	Con	*db/db*	Con	HFD	Con	Akita
Weight, g	23.1±0.25	42.3±0.20†	33.3±1.6	50.3±0.9†	24.6±0.5	23.1±0.5
Blood glucose, mg/dl	100.7±6.0	328.0±10.9†	05.5±5.5	125.1±4.1†	125.9±4.2	475.3±16.8†
Insulin, ng/ml	1.35±0.5	25.9±5.7†	3.6±1.1	28.0±6.9†	1.42±0.06	0.25±0.00†
IGF-I, ng/ml	659.9±19.9	764.1±41.5*	301.8±21.6	426.6±20.0†	416.4±21.4	415.8±17.9
FFA, mEq/l	0.78±0.04	1.68±0.11†	0.26±0.10	1.18±0.04	1.20±0.01	1.24±0.05
Ghrelin, fmol/ml	98.4±5.6	34.7±8.6†	164.9±7.5	67.2±10.6†	113.4±11.8	182.7±18.1†

Values are means ± SE. Con, control mice; HFD, mice on a high-fat diet; FFA, free fatty acids. *$P < 0.05$; †$P < 0.01$ compared with control mice or mice on a standard diet; $n = 7$.

Massy Cedes, France). Measurement of serum insulin concentrations was performed by ELISA using an ultrasensitive rat insulin kit (Morinaga, Yokohama, Japan). Serum insulin-like growth factor I (IGF-I) levels were measured using a mouse/rat IGF-I EIA kit (Diagnostic Systems Laboratories, Webster, TX). Serum free fatty acid (FFA) levels were measured by NEFA C test (Wako Pure Chemical Industries, Osaka, Japan).

Measurements of plasma ghrelin concentrations. Measurement of plasma ghrelin levels was performed as reported previously (12). Briefly, blood was drawn from the retroorbital vein after an overnight fast and then immediately transferred to chilled siliconized glass tubes containing Na_2EDTA (1 mg/ml) and aprotinin (1,000 KIU/ml; Ohkura Pharmaceutical, Kyoto, Japan) and centrifuged at 4°C. Immediately after the plasma was separated, hydrochloric acid was added to samples at final concentration of 0.1 N. Plasma was immediately frozen and stored at −80°C until assay. Plasma ghrelin concentrations were determined using an active ghrelin ELISA kit that recognizes *n*-octanoylated ghrelin (Mitsubishi Kagaku Iatron, Tokyo, Japan) (1).

Real-time quantitative RT-PCR. Total RNA was extracted from the pituitary and hypothalamus using a Sepasol RNA kit (Nacalai Tesque, Kyoto, Japan). Reverse transcription (RT) was performed in the presence of random hexamers with SuperScript II reverse transcriptase (Invitrogen, Carlsbad, CA). Real-time quantitative PCR was performed using an ABI PRISM 7500 Sequence Detection System (Applied Biosystems, Foster City, CA), using the following primers and TaqMan probes: mouse GH sense, 5′-AAGAGTTCGAGCGTGCCTACA-3′, and antisense, 5′-GAAGCAATTCCATGTCGGTTC-3′, with the TaqMan probe, 5′-CCATTCAGAATGCCCAGGCTGCTTTC-3′; mouse GHRH receptor (GHRH-R) sense, 5′-GCCCTTGGAACTGTTAACCA-3′, and antisense, 5′-GCAACCAGGATGGCAATAGC-3′, with the TaqMan probe, 5′-AGCATCTCCATTGTAGCCCTCTGCGTG-3′; mouse GHS-R sense, 5′-CACCAACCTCTACCTATCCAGCAT-3′, and antisense, 5′-CTGACAAACTGGAAGAGTTTGCA-3′, with the TaqMan probe, 5′-TCCGATCTGCTCATCTTCCTGTGCATG-3′; mouse ghrelin sense, 5′-GCATGCTCTGGATGGACATG-3′, and antisense, 5′-TGGTGGCTTCTTGGATTCCT-3′, with the TaqMan probe, 5′-AGCCCAGAGCACCAGAAAGCCCA-3′; mouse somatostatin receptor (SSTR)2 sense, 5′-GGTCAAGGCAGACAATTCACAA -3′, and antisense, 5′-GTGTTAGCACACATACACACAGGACTT -3′, with the TaqMan probe, 5′-CGGCAGAAACCGGAAAAACCAAAACTAAAT -3′; mouse SSTR5 sense, 5′-CGCTGCCTGACCGCTAAGTA-3′, and antisense, 5′-GCTCACAGAGGTTGGCTCACA-3′, with the TaqMan probe, 5′-CTGCACAGGAGAGGTCTCCACGGCT-3′; mouse GHRH sense, 5′-AGGATGCAGCGACACGTAGA-3′, and antisense, 5′-TCTCCCCTTGCTTGTTCATGA-3′, with the TaqMan probe, 5′-CCACCAACTACAGGAAACTCCTGAGCCA-3′. The mRNA expression in each gene was normalized to that of 18s ribosomal RNA.

Chronic administration of ghrelin and GHRH. Mice on a HFD (HFD mice) or a standard diet (control mice) for 20 wk were injected with 40 μg/kg ghrelin and 60 μg/kg GHRH twice daily for 10 days. Before and after treatment, blood samples were collected and body weights measured. Fat body mass and lean body mass of mice were measured by Latheta LTC-100 (Aloka, Tokyo, Japan) under pentobarbital anesthesia.

Statistical analysis. All values were expressed as means ± SE. The statistical significance of the differences in mean values was assessed by two-way ANOVA or Student's *t*-test as appropriate.

RESULTS

Basal profiles of *db/db*, HFD, and Akita mice are listed in Table 1. *Db/db* and HFD mice showed significantly higher weights, blood glucose, serum insulin, and serum IGF-I levels and significantly lower plasma ghrelin levels than those seen in control mice (Table 1), although the elevation of blood glucose was less severe in HFD mice. Although serum FFA levels of *db/db* mice were significantly higher than those of control mice, those of HFD mice were comparable with those of control mice (Table 1). Although Akita mice demonstrated significantly higher blood glucose levels as either *db/db* mice or HFD mice, Akita mice displayed significantly lower body weights and serum insulin levels and higher plasma ghrelin levels than those seen in control mice (Table 1).

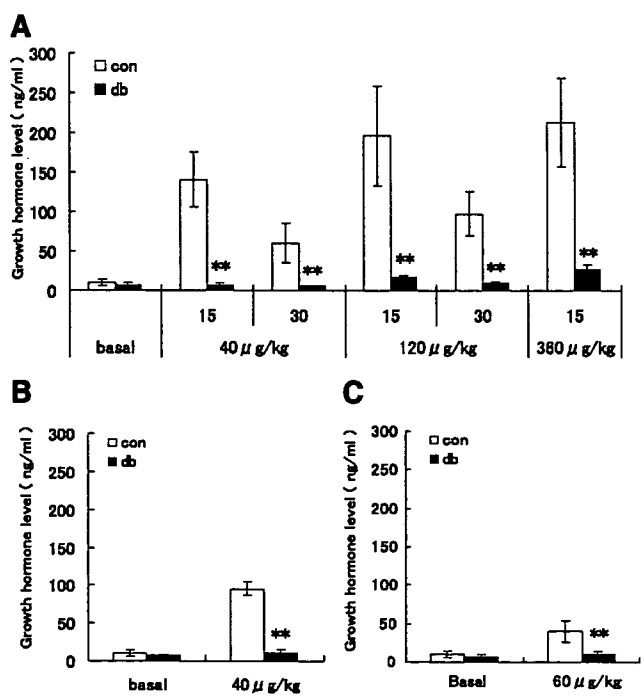

Fig. 1. Growth hormone (GH) responses to ghrelin in *db/db* mice. *A*: serum GH levels 15 or 30 min after sc injection of ghrelin into *db/db* (db) or control (con) mice. *B*: serum GH levels 15 min after iv ghrelin injection into db or con mice. *C*: serum GH levels 15 min after sc injection of GH-releasing hormone (GHRH). **$P < 0.01$.

We first examined acute GH responses to ghrelin in *db/db*, HFD, and Akita mice. GH responses to ghrelin in *db/db* mice were markedly lower than those observed in control mice at any dose (40, 120, or 360 μg/kg; Fig. 1*A*). Thirty minutes after ghrelin injection (40 or 120 μg/kg) of *db/db* mice, serum GH levels tended to be even lower than those at 15 min (Fig. 1*A*), indicating that low GH levels at 15 min were not due to delayed response. GH responses at 15 min after intravenous injection of ghrelin were also decreased in *db/db* mice (Fig. 1*B*), indicating that the disturbed GH responses observed in *db/db* mice were not due to the malabsorption of ghrelin caused by fat deposition at the subcutaneous injection site. GH responses to GHRH (60 μg/kg) were also decreased in *db/db* mice (Fig. 1*C*). As in *db/db* mice, GH levels at 15 min after subcutaneous ghrelin injection (40, 120, and 360 μg/kg) in HFD mice were significantly lower than those seen in control mice (Fig. 2*A*). GH responses to GHRH (60 μg/kg) also tended to be decreased (Fig. 2*B*). Although GH levels in Akita mice were not significantly different from those in control mice measured at 15 min after 40 μg/kg sc injection of ghrelin, those measured after a higher dose of ghrelin (120 and 360 μg/kg) were significantly lower than those in control mice (Fig. 3*A*). GH responses to GHRH (60 μg/kg) also tended to be decreased in Akita mice (Fig. 3*B*).

We then measured 1-h food intake stimulated by ghrelin in *db/db* and Akita mice. In control mice, a 40 μg/kg sc ghrelin injection evoked about threefold greater food intake than that induced by saline injection (saline vs. ghrelin: 0.09 ± 0.04 vs. 0.28 ± 0.01 g, $P < 0.05$, $n = 7$; Fig. 4*A*). Ghrelin stimulated additional food intake in a dose-dependent manner in control mice, as demonstrated by the ratio of food intake evoked by ghrelin to that induced by saline (Fig. 4*A*). In *db/db* mice, basal food intake was higher than that of control mice (0.22 ± 0.05 vs. 0.07 ± 0.02 g, $P < 0.05$, $n = 7$). Although sc injection of 40 μg/kg ghrelin into *db/db* mice did not stimulate food intake significantly (saline vs. ghrelin: 0.30 ± 0.11 vs. 0.18 ± 0.04 g, $P = 0.30$, $n = 7$), higher doses of ghrelin (360 μg/kg), however, were able to stimulate food intake (saline vs. ghrelin: 0.14 ± 0.08 vs. 0.39 ± 0.04 g, $P < 0.05$, $n = 7$). Although higher ghrelin stimulated food intake in *db/db* mice, the extent of stimulation as demonstrated by the ratio of ghrelin-induced food intake (40 and 360 μg/kg) to that by saline was significantly smaller than that in control mice (Fig. 4*A*). In Akita mice, basal food intake was higher than that of control mice (0.28 ± 0.01 vs. 0.15 ± 0.02 g, $P < 0.05$, $n = 7$), and no further stimulation of food intake by ghrelin was observed (Fig. 4*B*).

We then measured the mRNA expression of ghrelin-GH system in pituitaries and hypothalamuses of *db/db*, HFD, and Akita mice (Fig. 5). Pituitary mRNA levels of GHS-R were significantly lower in *db/db* and HFD mice, whereas those in Akita mice were significantly higher compared with their

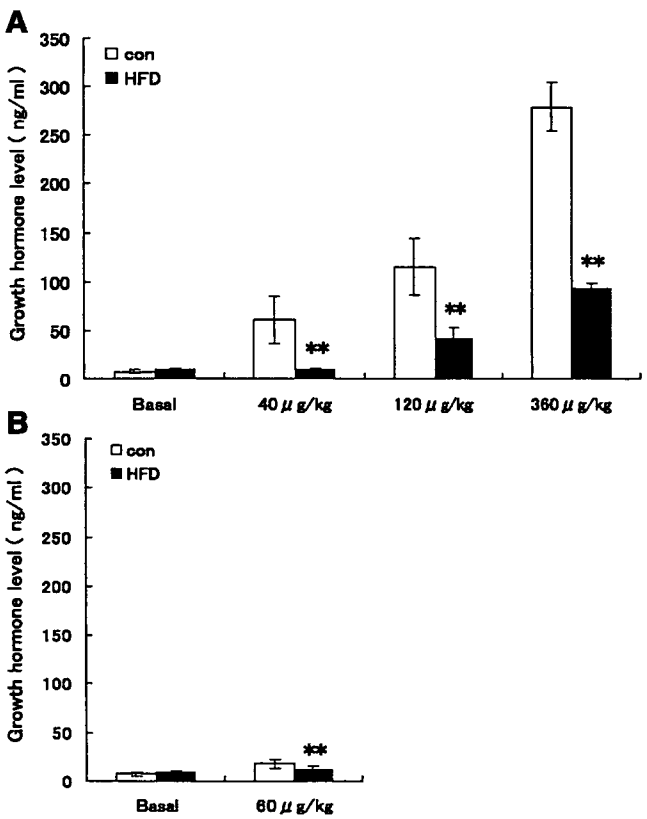

Fig. 2. GH responses to ghrelin in a diet-induced obesity mouse model. *A*: serum GH levels 15 min after sc injection of ghrelin into mice on a high-fat diet (HFD) or con mice. *B*: serum GH levels 15 min after GHRH sc injection. $^{**}P < 0.01$ compared with controls; $n = 7$.

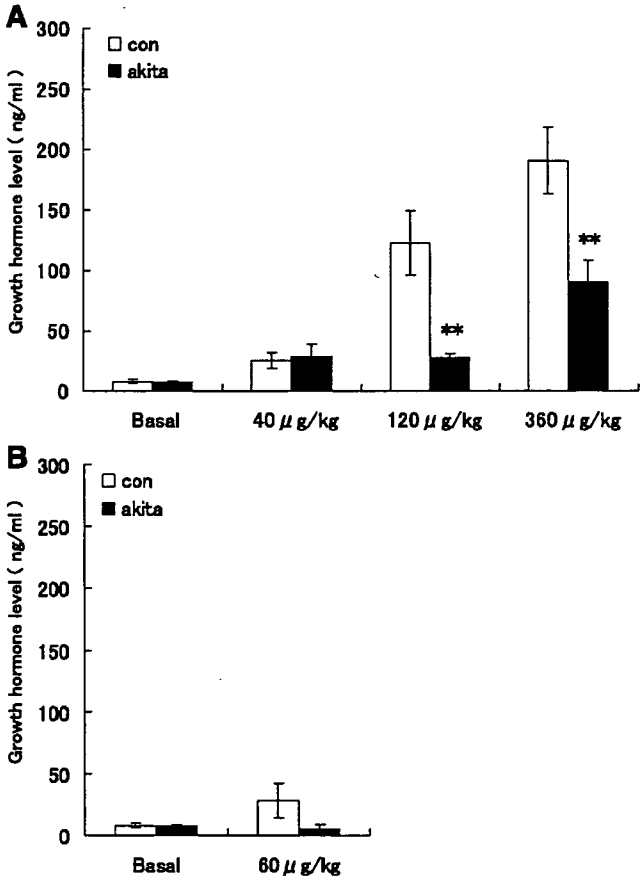

Fig. 3. GH responses to ghrelin in Akita mice. *A*: serum GH levels 15 min after sc injection of ghrelin into Akita or con mice. *B*: serum GH levels 15 min after sc injection of GHRH. $^{**}P < 0.01$ compared with control; $n = 7$.

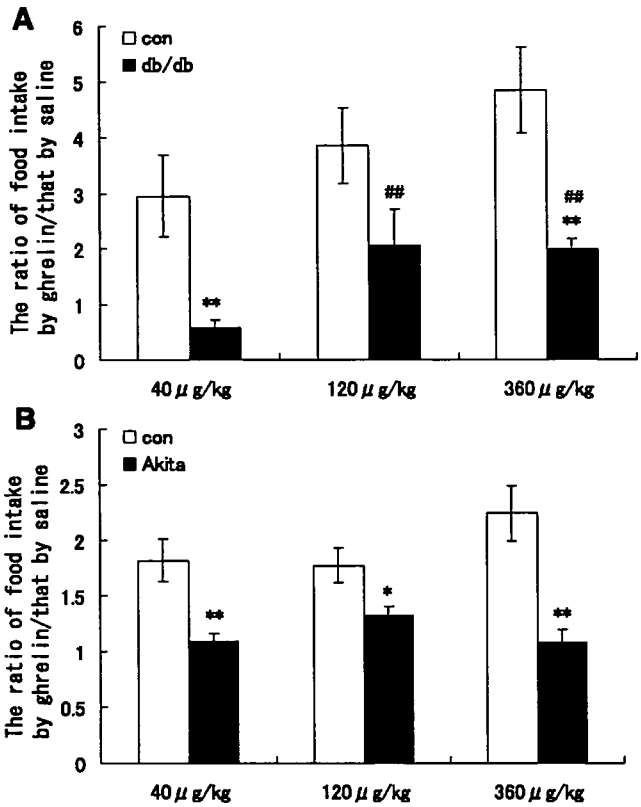

Fig. 4. Food intake stimulated by sc ghrelin injection. *A*: the ratio of 1-h food intake after sc ghrelin injection to that observed after sc saline injection in db and con mice. *B*: the ratio of the food intake observed for 1 h after sc ghrelin injection to that seen after saline injection for Akita and con mice. $*P < 0.05$; $**P < 0.01$ compared with control; $\#\#P < 0.01$ compared with 40 μg/kg; $n = 7$.

control mice (Fig. 5*A*). Pituitary mRNA levels of ghrelin were significantly lower in *db/db* mice, whereas those in Akita mice were significantly higher (Fig. 5*A*). Pituitary mRNA levels of GH were significantly lower in *db/db* and HFD mice and tended to be lower in Akita mice (Fig. 5*A*). Pituitary mRNA levels of SSTR2 were significantly higher in *db/db* mice, whereas they were not significantly changed in HFD and Akita mice (Fig. 5*A*). Pituitary mRNA levels of SSTR5 were significantly lower in Akita mice, whereas those levels were not significantly changed in *db/db* and HFD mice (Fig. 5*A*). There were no significant changes in the expression levels of GHRH-R in pituitaries of these mice (Fig. 5*A*). In hypothalamus, GHS-R and GHRH mRNA levels were significantly higher and lower, respectively, in Akita mice (Fig. 5*B*). Ghrelin mRNA levels were significantly lower in hypothalamus of HFD mice (Fig. 5*B*).

Finally, we examined the effect of chronic ghrelin injection to HFD mice. To maximize GH-stimulating activity of ghrelin and to minimize orexigenic action of ghrelin, we first examined GH responses to low-dose ghrelin with GHRH coadministration in HFD mice. Acute GH responses to ghrelin were significantly potentiated by coadministration of GHRH even at the lowest dose in HFD mice (Fig. 6*A*). By 10 days of twice daily injections of saline or ghrelin and GHRH, both control and HFD mice lose weight by ~6–8%. This weight reduction might be due to stress of twice daily injection, which is usually covered by growth in younger mice. Control mice treated with ghrelin and GHRH tended to take in more food than those with saline (Fig. 6*C*). Fat masses were more preserved in the ghrelin- and GHRH-treated groups than in the saline-treated group in control mice (Fig. 6, *B*, *D*, and *E*), although percent body weight and percent lean body mass changes were comparable between the saline-treated and the ghrelin- and GHRH-treated group in control mice. In HFD mice, food intake, percent body weight change, and percent lean body mass change were comparable between the saline-treated group and the ghrelin- and GHRH-treated groups (Fig. 6, *B*, *D*, and *E*). In contrast to control mice, fat mass tended to even be decreased in the ghrelin and GHRH group than in the saline-treated group in HFD mice (Fig. 6*D*). In both control and HFD mice, blood glucose, serum insulin, and serum IGF-I levels of the ghrelin- and GHRH-treated group were not significantly different from those of the saline-treated group (Fig. 6, *F*, *G*, and *H*).

DISCUSSION

We have demonstrated that GH responses to ghrelin are decreased in both genetic and diet-induced mouse models of obesity. Recently, Luque and Kineman (15) reported that plasma GH levels acquired by random sampling without stimulation in *ob/ob* mice and HFD mice tended to be lower than

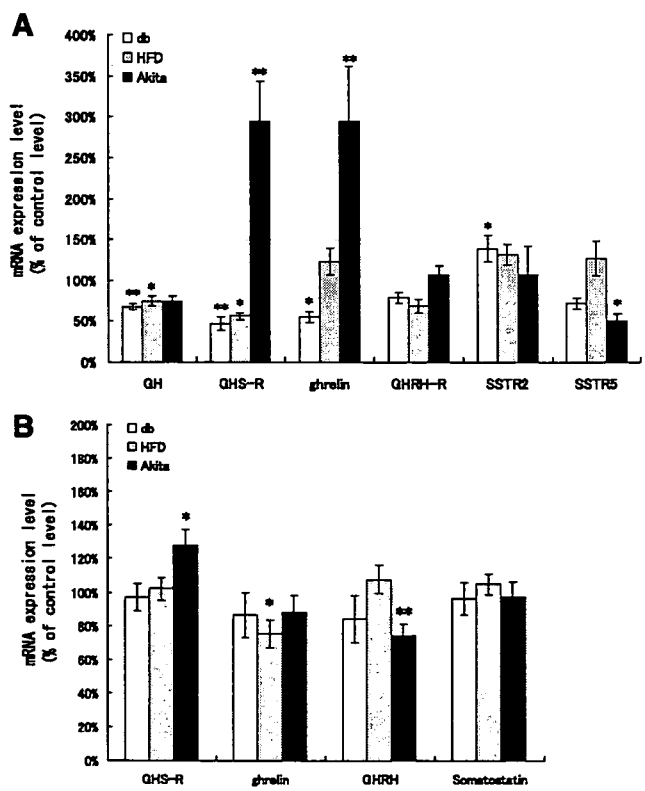

Fig. 5. The mRNA expression levels in the pituitaries or hypothalamuses of db mice, mice on a HFD, and Akita mice. *A*: the mRNA expression levels of GH, GH secretagogue receptor (GHS-R), ghrelin, GH-releasing hormone receptor (GHRH-R), somatostatin receptor (SSTR)2, and SSTR5 in the pituitaries of db, HFD, and Akita mice. *B*: the mRNA expression levels of GHS-R, ghrelin, GHRH, and somatostatin in the hypothalamuses of db, HFD, and Akita mice. Data were presented as % of the level seen in control mice. $*P < 0.05$; $**P < 0.01$ compared with control; $n = 14$.

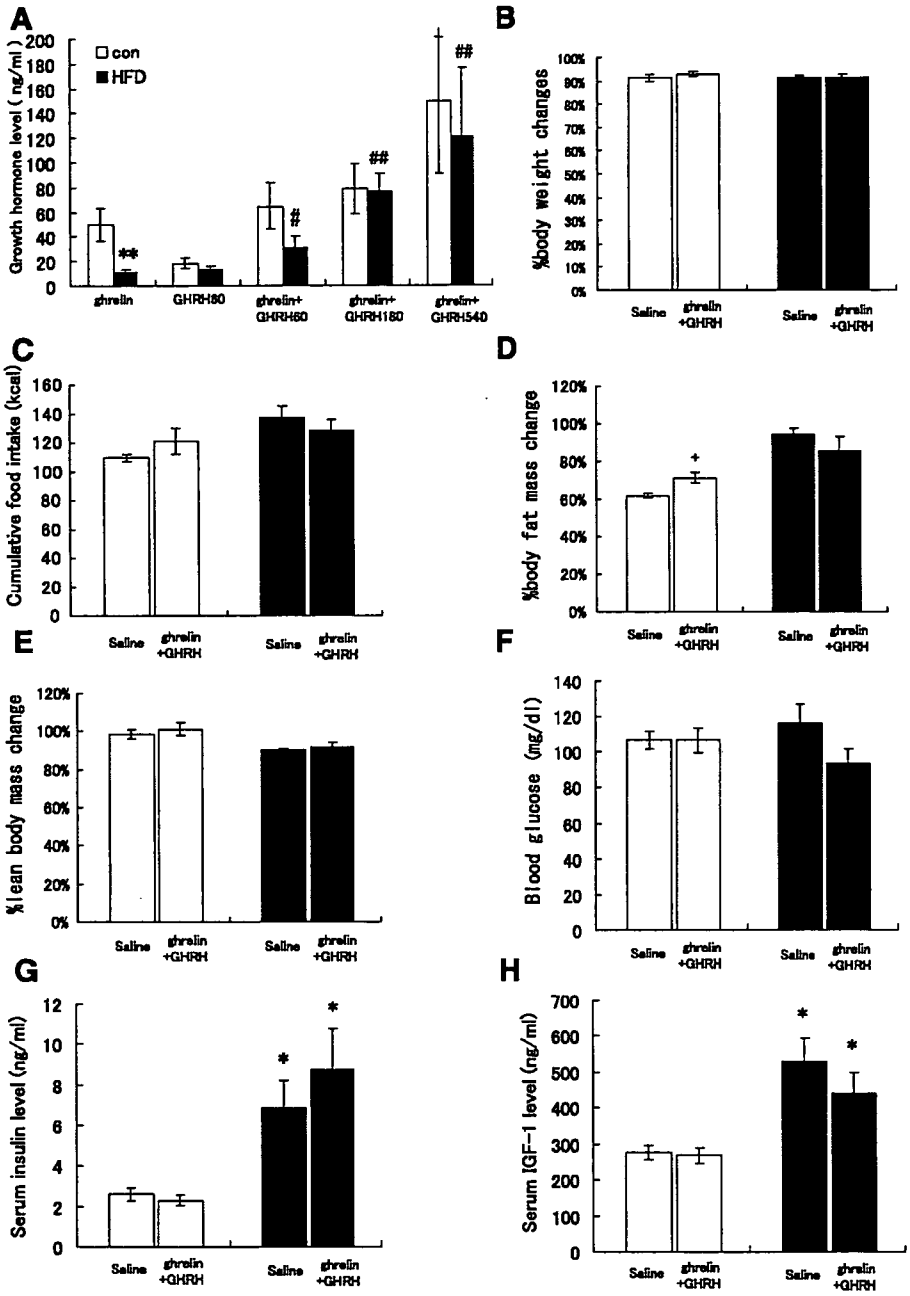

Fig. 6. Chronic treatment of ghrelin and GHRH on mice on a HFD. *A*: serum GH levels 15 or 30 min after sc injection of 40 μg/kg ghrelin or 60 μg/kg GHRH or ghrelin and GHRH (60, 180, 540 μg/kg) into HFD or con mice. %Body weight (*B*), fat mass (*D*), and lean body mass (*E*) changes before and after treatment of 40 μg/kg ghrelin and 60 μg/kg GHRH or saline for 10 days in control mice (open bars) or mice on a HFD (filled bars). *C*: cumulative food intake for 10 days. Blood glucose (*F*), serum insulin level (*G*), and serum IGF-I level (*H*) after 10 days administration of ghrelin and GHRH. $*P < 0.05$; $**P < 0.01$ compared with control; $\#P < 0.05$; $\#\#P < 0.01$ compared with ghrelin; $+P < 0.05$ compared with saline; $n = 7$.

those seen in control mice. Because GH secretion is pulsatile, it is difficult to compare GH values obtained by random sampling in the absence of stimulation. For this reason, we could not detect any significant difference in basal GH values between *db/db* or HFD and control mice. Following ghrelin or GHRH stimulation, however, we clearly observed a severe impairment in GH secretions by obese mice. Alvarez-Castro et al. (2) previously reported that GH responses to ghrelin were decreased in obese human subjects compared with those seen in normal controls; although reduced, these responses to ghrelin were greater in magnitude than those observed following GHRH treatment in obese human subjects. Our observations in mice were consistent with these data obtained in humans, which verify the use of *db/db* and HFD mice as experimental animal models for ghrelin treatment for obesity.

We also demonstrated that GH responses to ghrelin are decreased in Akita mice. As far as we know, this is the first report on the GH responses to ghrelin in insulin-deprived mice. In humans with insulin-deprived diabetes, it is well known (11) that basal GH is elevated and that GH response to provocative tests, including GHRH or GHS administration, is exaggerated. Thus discrepancy between human and mouse GH response to ghrelin in insulin-deprived status exist.

We demonstrated that GHS-R mRNA levels were decreased in the pituitaries of *db/db* and HFD mice. Ghrelin does stimulate GH release from rat pituitary in vitro (14), but maximal